



# Mid- to late Pliocene (3.3–2.6 Ma) global sea-level fluctuations recorded on a continental shelf transect, Whanganui Basin, New Zealand

G.R. Grant<sup>a,\*</sup>, J.P. Sefton<sup>b</sup>, M.O. Patterson<sup>c</sup>, T.R. Naish<sup>a</sup>, G.B. Dunbar<sup>a</sup>, B.W. Hayward<sup>d</sup>, H.E.G. Morgans<sup>e</sup>, B.V. Alloway<sup>f,g</sup>, D. Seward<sup>h</sup>, C.A. Tapia<sup>i</sup>, J.G. Prebble<sup>e</sup>, P.J.J. Kamp<sup>j</sup>, R. McKay<sup>a</sup>, C. Ohneiser<sup>k</sup>, G.M. Turner<sup>l</sup>

<sup>a</sup> Antarctic Research Centre, Victoria University of Wellington, PO Box 600, Wellington 6012, New Zealand

<sup>b</sup> Department of Geography, Durham University, South Road, Durham, DH1 3LE, United Kingdom

<sup>c</sup> Binghamton University, State University of New York, 4400 Vestal Parkway East, Binghamton, NY 13902, USA

<sup>d</sup> Geomarine Research, 19 Debron Ave, Remuera, Auckland, New Zealand

<sup>e</sup> GNS Science, 1 Fairway Drive, Avalon 5010, PO Box 30-368, Lower Hutt 5040, New Zealand

<sup>f</sup> School of Environment, University of Auckland, Private Bag 92019, Auckland 1142, New Zealand

<sup>g</sup> Centre for Archaeological Science (CAS), University of Wollongong, Wollongong, NSW 2522, Australia

<sup>h</sup> School of Geography, Environment and Earth Sciences, Victoria University of Wellington, PO Box 600, Wellington 6012, New Zealand

<sup>i</sup> Department of Civil Works and Geology, Faculty of Engineering, Catholic University of Temuco, Avenida Alemania No. 0211, Casilla 15-D, Temuco, Chile

<sup>j</sup> School of Science, University of Waikato, Hamilton 3240, New Zealand

<sup>k</sup> Department of Geology, University of Otago, PO Box 56, Dunedin, 9054, New Zealand

<sup>l</sup> School of Chemical and Physical Sciences, Victoria University of Wellington, PO Box 600, Wellington 6012, New Zealand

## ARTICLE INFO

### Article history:

Received 18 May 2018

Received in revised form

2 August 2018

Accepted 28 September 2018

Available online 25 October 2018

## ABSTRACT

We present a ~900 m-thick, mid- (3.3–3.0 Ma) to late Pliocene (3.0–2.6 Ma), shallow-marine, cyclical sedimentary succession from Whanganui Basin, New Zealand that identifies paleobathymetric changes, during a warmer-than-present interval of Earth history, relevant to future climate change. Our approach applies lithofacies, sequence stratigraphy and benthic foraminiferal analyses to two continuously-cored drillholes integrated with new and existing outcrop studies. We construct a depositional model of orbitally-paced, global sea-level changes on a wave-graded continental shelf. Unlike many previous studies, these shelf sediments were not eroded during sea-level lowstands and thus provide the potential to reconstruct the full amplitude of glacial-interglacial sea-level change. Paleobathymetric interpretations are underpinned by analysis of extant benthic foraminiferal census data and a statistical correlation with the distribution of modern taxa. In general, water depths derived from foraminiferal Modern Analogue Technique (MAT), are consistent with variability recorded by lithofacies.

The inferred sea-level cycles co-vary with a qualitative climate record reconstructed from a census of extant pollen and spores, and a modern temperature relationship. A high-resolution age model is established using magnetostratigraphy constrained by biostratigraphy, and the dating and correlation of tephra. This integrated chronostratigraphy allows the recognition of 23 individual sedimentary cycles, that are correlated across the paleo-shelf and a possible “one-to-one” relationship is made to deep-ocean benthic oxygen isotope ( $\delta^{18}\text{O}$ ) records. In general water depth changes were paced by ~20 kyr duration between 3.3 and 3.0 Ma, after which cycle duration is ~40 kyr during the late Pliocene (3.0–2.6 Ma). This record provides a future opportunity to evaluate the amplitude and frequency of global, Pliocene glacio-eustatic sea-level change, independent of the global benthic  $\delta^{18}\text{O}$  record.

© 2018 Elsevier Ltd. All rights reserved.

\* Corresponding author.

E-mail address: [georgia.grant@vuw.ac.nz](mailto:georgia.grant@vuw.ac.nz) (G.R. Grant).

## 1. Introduction

### 1.1. Pliocene climate and sea-level change

The mid- to late Pliocene (3.3–2.6 Ma) spans one of the most significant climatic transitions of the Cenozoic. It is characterised by global cooling from a climate with an atmospheric CO<sub>2</sub> concentration of ~400 ppm and temperature of 2–3 °C warmer-than-present (summarised in [Masson-Delmotte et al., 2013](#)), to one marked by the progressive expansion of ice sheets on northern hemisphere continents (e.g. [Raymo, 1994](#)) as CO<sub>2</sub> fell below 300 ppm ([DeConto et al., 2008](#)). Consequently, the mid-Pliocene warm period (3.3–3.0 Ma) provides the most accessible and recent geological analogue for global sea-level variability relevant to future warming.

Pliocene sea-level changes have been reconstructed using a variety of geological techniques, including benthic  $\delta^{18}\text{O}$  records and Mg/Ca paleothermometry, submerged coral reefs, the relationship between water-depth and salinity in the Red Sea ([Rohling et al., 2014](#)) and backstripped continental margins ([Miller et al., 2012](#) and refs. therein). Although there are considerable uncertainties with all these techniques, a central value for peak global mean sea-level (GMSL), during the mid-Pliocene centred on  $\sim 20 \pm 10$  m (above present day), has become widely accepted ([Miller et al., 2012](#); [Dutton et al., 2015](#)).

However, it now appears that estimating the absolute magnitude of peak Pliocene GMSL, with respect to present day, is beyond our current capability due to Earth deformation processes. Global mantle dynamic processes ([Moucha et al., 2008](#); [Müller et al., 2008](#)) could contribute more than  $\pm 10$  m to the uncertainty when reconstructing paleo sea-level. Visco-elastic response of the crust and gravitational changes (glacio-isostatic adjustment; GIA) associated with the redistribution of water between ice sheets and the oceans can cause deviations from GMSL on the order of 5–30 m for sites in the far and near fields of ice sheets respectively ([Raymo et al., 2011](#)). Consequently, both GIA and dynamic topography signals can be as large as the sea-level estimate itself and current estimates of their amplitudes carry large uncertainties.

While benthic  $\delta^{18}\text{O}$  records provide the most detailed and well-dated proxy of climate variability during the Pliocene and Pleistocene (e.g. [Lisiecki and Raymo, 2005](#)), their signal reflects ocean temperature and ice volume. Calibration of the ice volume component of the  $\delta^{18}\text{O}$  record using sea-level reconstructions from far-field shallow-marine continental margins ([Naish, 1997](#); [Miller et al., 2005](#); [Naish and Wilson, 2009](#); [Miller et al., 2012](#)) is also complicated by uncertainties and assumptions. Backstripping approaches to date have uncertainties resulting from the broad depth ranges inherent to faunal paleodepth indicators. An additional impediment is that in many cases sea-level lowstand unconformities result in incomplete records which hinders determination of full amplitude sea-level variability.

Notwithstanding this, far-field shallow-marine continental margins are less affected by GIA, and have the potential to capture the full amplitude of global sea-level changes on glacial-interglacial time-scales (e.g. [Naish and Wilson, 2009](#); [Miller et al., 2012](#)). Moreover, mantle dynamic processes are negligible at orbital timescales. If a more precise paleobathymetry can be reconstructed (e.g. [Dunbar and Barrett, 2005](#)), then a backstripping approach would produce a relative sea-level curve. Such a curve would be independent of the  $\delta^{18}\text{O}$  record that will allow the uncertainties in the  $\delta^{18}\text{O}$  record to be assessed.

Suitable continental margins require shallow-marine, sedimentary basins with high sedimentation rates ( $>1$  m/kyr), where accommodation space (subsidence rate) has been sufficient to prevent shallow-marine or subaerial erosion during sea-level

lowstands. This type of depositional setting can be a very sensitive recorder of multi-metre-amplitude, cyclic changes in water depth.

Such sedimentary basins are rare, but do occur on convergent plate margins (e.g. Italy, Japan, New Zealand). Whanganui Basin, New Zealand, comprises one of the highest-resolution, shallow-marine records of orbitally-paced, late Neogene global sea-level change (e.g. [Naish et al., 1998](#)). Its ~5 km thick, composite sedimentary-fill ([Fleming, 1953](#); [Anderton, 1981](#)) accumulated as a consequence of relatively linear rate of basin subsidence due to plate boundary interactions behind the Hikurangi subduction zone off eastern New Zealand ([Stern et al., 1992](#), [Fig. 1](#)). Sediment deposition in the basin has more-or-less kept pace with the rate of accommodation creation through the past 5 Ma (e.g. [Naish et al., 1998](#); [Saul et al., 1999](#)).

### 1.2. Aims of this paper

In this paper, we report on two new sediment cores (Siberia-1 and Tiriraukawa-1) that recovered a continuous and high-resolution (~1 m/kyr sedimentation rate) succession of cyclical environmental change from laterally adjacent outer to middle shelf environments, in Whanganui Basin, New Zealand. In contrast to Pleistocene-age cycles from Whanganui Basin, these have not been eroded during sea-level lowstands. These cores, together with regional outcrop stratigraphy, provide the opportunity to fully resolve glacial-interglacial sea-level changes between 3.3 and 2.6 Ma.

The approach applied here involves a sedimentological description, down-core physical property measurements, and grainsize analysis to support a sedimentary facies interpretation of environmental change. We establish water depth changes using statistical analysis of extant benthic foraminiferal census data and Modern Analogue Technique (MAT) to reconstruct paleobathymetry of the continental shelf transect (e.g. [Hayward et al., 1999](#); [Hayward and Triggs, 2016](#)). Sequence architecture across the SE-NW deepening wave-graded paleo-shelf transect allows the lateral sedimentary expression of cyclical bathymetric changes to be evaluated in the context of changes in sediment supply, basin subsidence and sea-level change.

Finally, we present an integrated age model, developed from magnetostratigraphy ([Tapia et al., 2018](#), in review), biostratigraphy and tephrochronology. Correlation of the sedimentary cycles identified within the two drill cores with cycles in other regional outcrop successions ([Fig. 1](#)) in the Rangitikei River Section ([Kamp et al., 1998](#); [Turner et al., 2005](#)), Turakina River Section ([Turner et al., 2005](#); [Patterson, 2014](#)) and Watershed Road Section ([Sefton, 2015](#)), constrained by the new chronostratigraphic framework, enables orbital-scale, glacial-interglacial changes of water depth to be determined. We discuss the potential application of the new drill cores for quantitative reconstruction of the frequency and amplitude of global mean-sea-level change between 3.3 and 2.6 Ma, independent of the global benthic  $\delta^{18}\text{O}$  stack ([Lisiecki and Raymo, 2005](#)).

## 2. Geologic setting

The Whanganui Basin ([Fig. 1](#)) in western North Island is located southwest of an active volcanic arc (Taupo Volcanic Zone), and west of the accretionary prism that forms the leading edge of the over-riding part of the Hikurangi Margin, where the oceanic Pacific Plate is subducting below continental crust of the Indo-Australian Plate (e.g., [Kamp et al., 2004](#)). The basin's depocentre has migrated southwards since the Miocene at ~30 mm/yr from the King Country to the presently subsiding river valleys in the North Marlborough

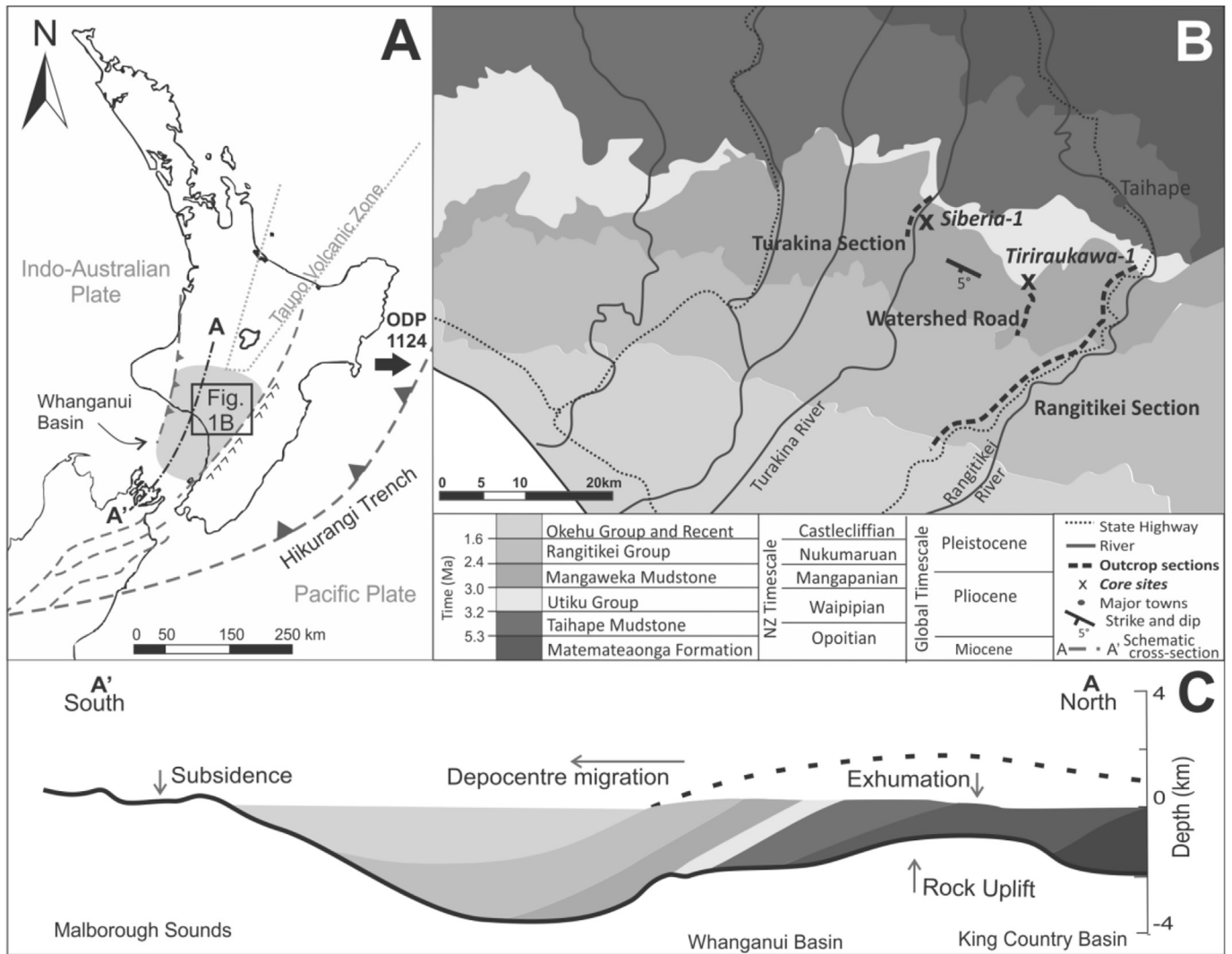


**Fig. 1.** a) Location map of Whanganui Basin in relation to the Pacific and Indo-Australian Plate boundary (Hikurangi Trench). ODP site 1124 lies ~500 km offshore to the northeast of Wellington. b) The location of the cores (Siberia-1 and Tiriraukawa-1; this study) and outcrop sections (Turakina: Patterson, 2014, Watershed Road: Sefton, 2015 and Rangitikei: Journeaux et al., 1996; Kamp et al., 1998) are shown on the geological map with formation names and both the New Zealand stage names and international epochs noted. Strata generally dip at 5° southwest. c) The A – A' schematic cross-section conceptually illustrates the southward migration of the depocentre and contemporaneous uplift in the north, exposing the geological units onshore (after Stern et al., 2013).

region (Fig. 1c), as a topographic wave in response to redistribution of lithosphere over the mantle (Stern et al., 2013). Consequently, the position of the paleo-shoreline during deposition of the mid- to late Pliocene sediments was controlled by the southwest passage of the east-west trending tectonic hinge line. Paleogeographic reconstructions (Bunce et al., 2009; Treweek and Bland, 2012) describe a broad west-facing marine embayment with an arcuate shoreline running along the north and western boundary, and exposed basement forming the ranges along its eastern margin (Fig. 2). Progressive uplift to the northeast and subsidence to the southwest has resulted in southward tilting of the strata on the order of 3–15° to the southwest (Stern et al., 2013; Naish and Kamp, 1995; Journeaux et al., 1996). Additional influences arising from local isostatic rebound from subsequent erosion of over 2000 m of exhumed material, exacerbated the uplift of the basin to the north (Pulford and Stern, 2004).

Previous attempts to reconstruct the amplitude of sea-level changes in Pliocene shallow-marine cycles have been made from outcrops in the shallower eastern margin of the basin (Rangitikei River Section; Fig. 1b). However, these sediments accumulated in

inner shelf to shoreline water depths, punctuated by erosional unconformities formed during glacial sea-level lowstands (Naish, 1997; Naish and Wilson, 2009). Accordingly, the sea-level estimates could only constrain minimum amplitudes.

This paper addresses the mid- to late Pliocene (3.3–2.6 Ma) part of the stratigraphic succession exposed in the basin between the Rangitikei and Turakina Rivers (Fig. 1).

### 3. Stratigraphic framework

The Pliocene succession has been subdivided into three broad lithostratigraphic units, which display higher order sedimentary cyclicity (Journeaux et al., 1996; Naish and Kamp, 1995):

- Upper part of the Tangahoe Formation deposited on the upper slope and outer shelf during the earliest part of the Waipipian Stage (early Pliocene, ~3.7–3.2 Ma);
- The Utiku Group deposited on the outer to inner shelf during the late Waipipian Stage (mid-Pliocene; ~3.2–3.0 Ma);

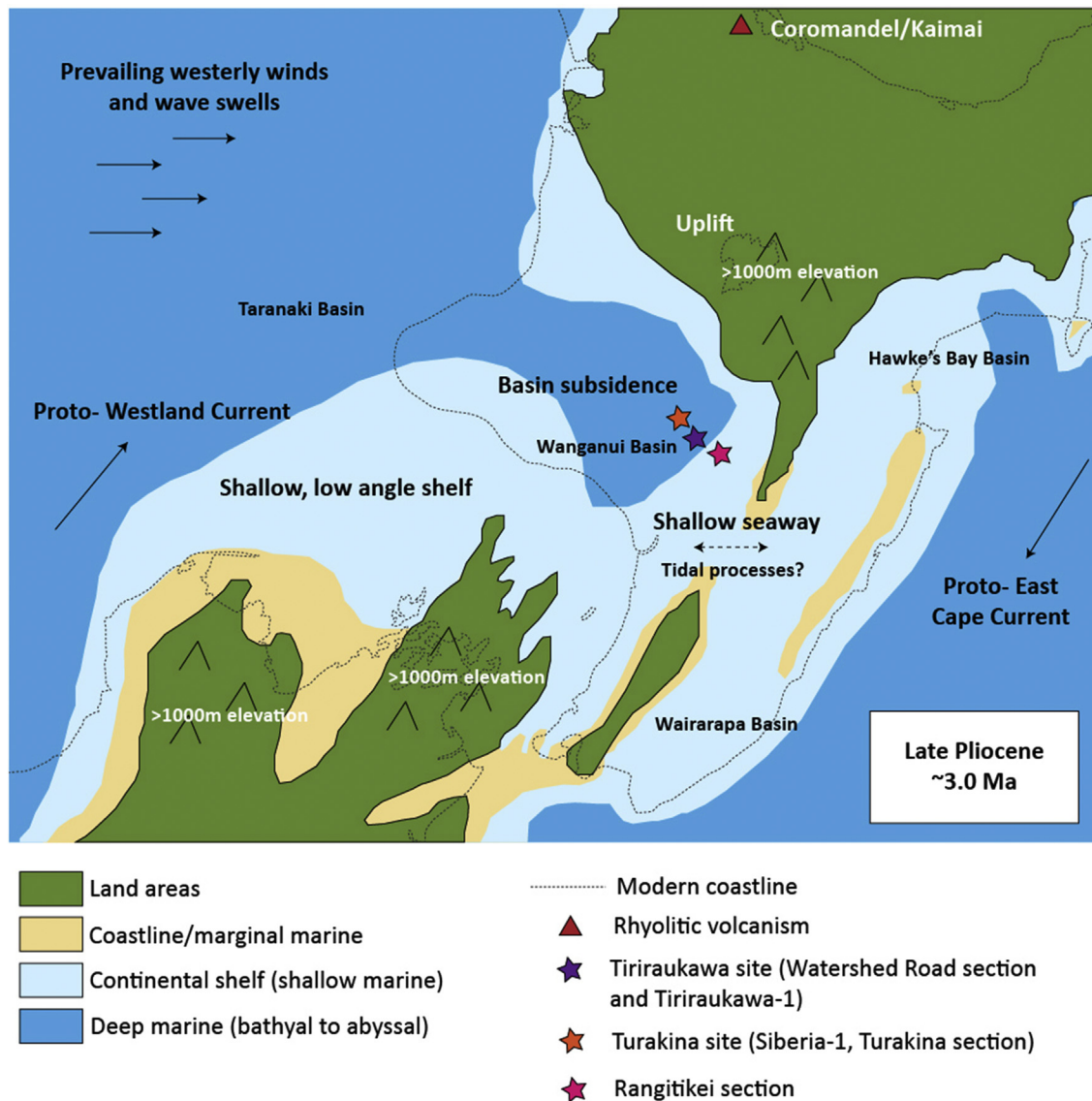


**Fig. 2.** A simplified paleogeographic reconstruction after Bunce et al. (2009) and Trewick and Bland (2012), displaying a semi-enclosed embayment open to the dominant westerly wind, with an arcuate shoreline and a deepening shelf westward. Continental shelf (0–200 m) and deep marine (>200 m) are approximate. The location of outcrop sections and cores shown in Fig. 1 are indicated.

- (iii) Mangaweka Mudstone deposited on the outer to middle shelf during the Mangapanian Stage (late Pliocene, ~3.0–2.6 Ma).

Sediments forming the ~350 m-thick Utiku Group deepen laterally to the west across the basin starting at middle and inner shelf depths in the Rangitikei River Section and deepening to outer and middle shelf depths in the Turakina River Section. A regional subsidence event marks an abrupt deepening in the Rangitikei River Section at the top of the Utiku Group from inner shelf (50 m) to outer shelf (>100 m) depths, possibly in response to southward migration of the depocentre (Kamp et al., 1998). The overlying Mangaweka Mudstone was deposited in outer to middle shelf depths in the Rangitikei River Section and deepens west across the study area where it was deposited in an outer shelf to upper slope environment.

The two drill sites were targeted to recover age-equivalent, continuous records of mid-Pliocene strata, from different locations on a westward deepening paleo-shelf transect. The sites were

chosen to avoid missing section due to lowstand erosion that characterises the Rangitikei River Section.

### 3.1. Siberia-1 drill core

Siberia-1 was spudded in July 2014, at Siberia Station 300 m east of the Turakina River (S39.6964° E175.5241°) into the lowermost part of the Mangaweka Mudstone (Fig. 1). It was cored continuously to a depth of 352 m with the exception of the upper 40 m, which was poorly-recovered unconsolidated recent colluvium. The recovered stratigraphic record contains 13 full sedimentary cycles, ranging from 10 to 50 m in thickness, within the Utiku Group that spans a downhole interval between 40 and 276 m. The cycles are characterised by oscillations in grain size from 10 to 60% sand, and lithologic changes ranging from clay-rich mudstone and mudstone to fine-sandy mudstone/muddy sandstone (Fig. 3a). Cycle boundaries are conformable and correspond to the inferred shallowest paleobathymetry as expressed by maximum sand percentage. Physical properties logs of the borehole and the core also co-vary



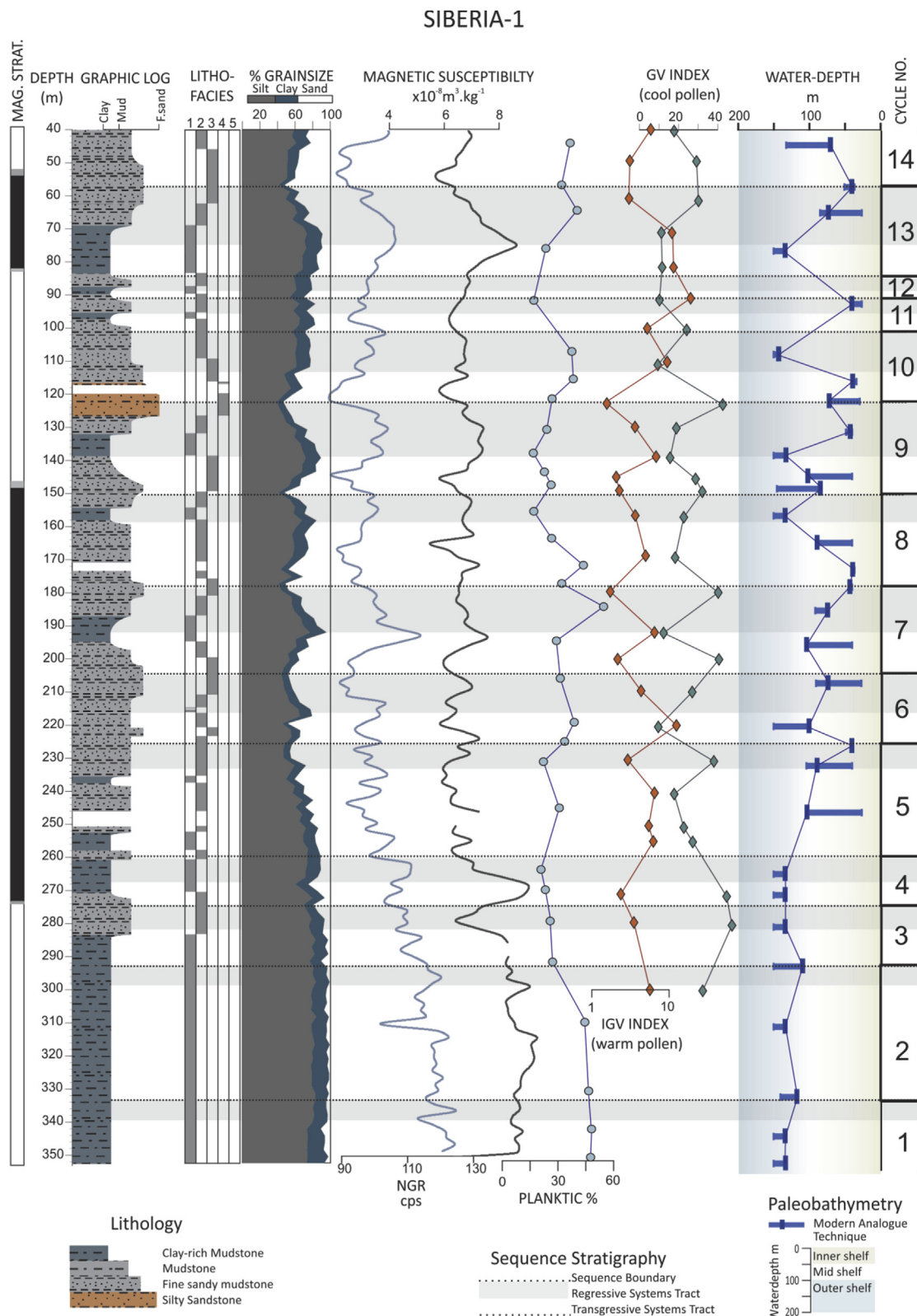


**Fig. 3.** (a) Siberia-1 and (b) Tiriraukawa-1 drill core showing core magnetostratigraphy (black: normal; white: reversal; grey: uncertain) and stratigraphy, lithofacies, clay/silt/sand percentage, natural gamma-ray (NGR) and magnetic susceptibility physical property logs, planktic foraminiferal percentage and palynological glacial-interglacial indices (for Siberia-1 only). Water depths derived by the benthic foraminiferal MAT (outlined in section 5.2) are displayed as mean values (dark blue rectangle) and minimum and maximum values (light blue bar). (For interpretation of the references to colour in this figure legend, the reader is referred to the Web version of this article.)

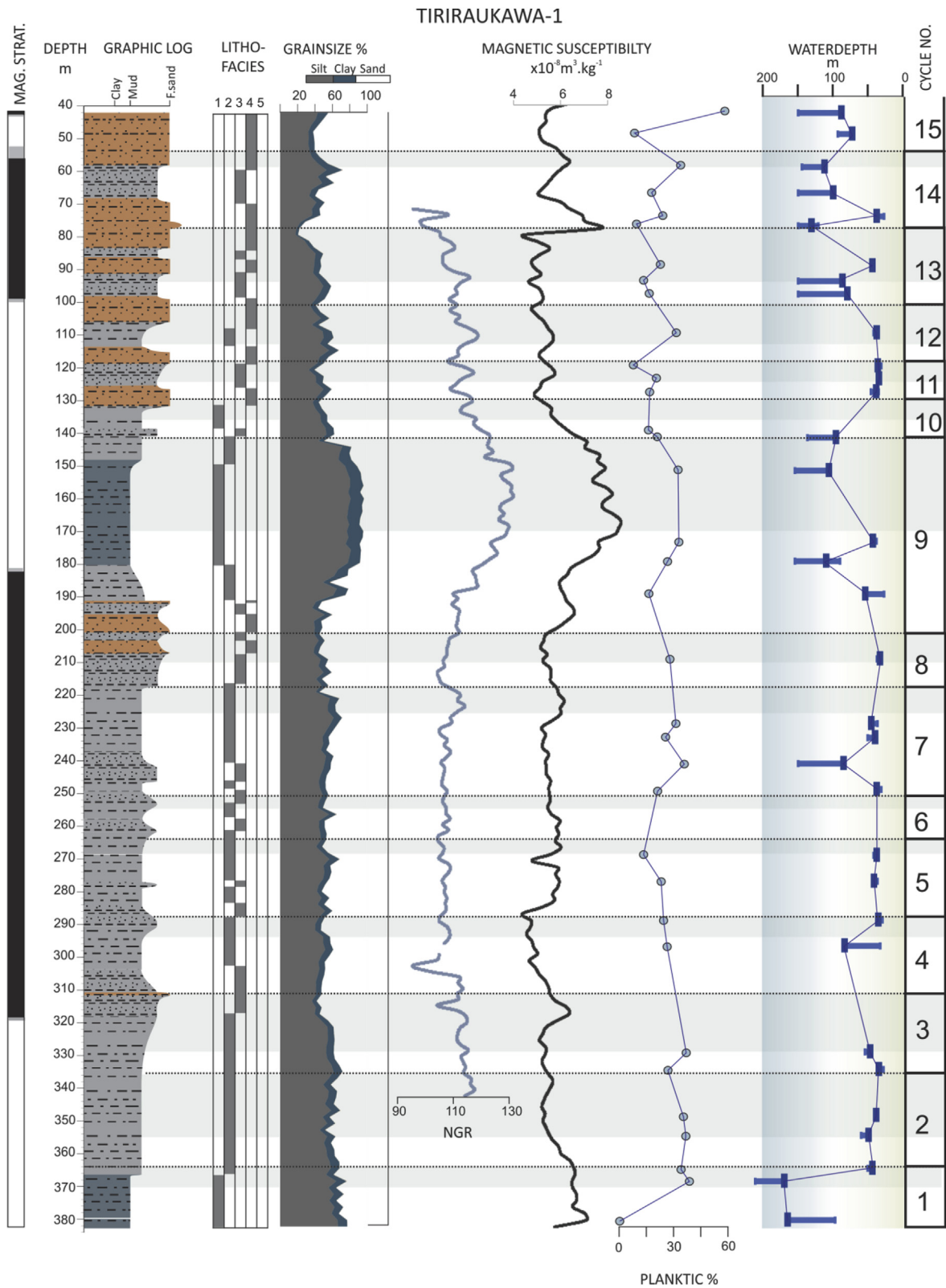
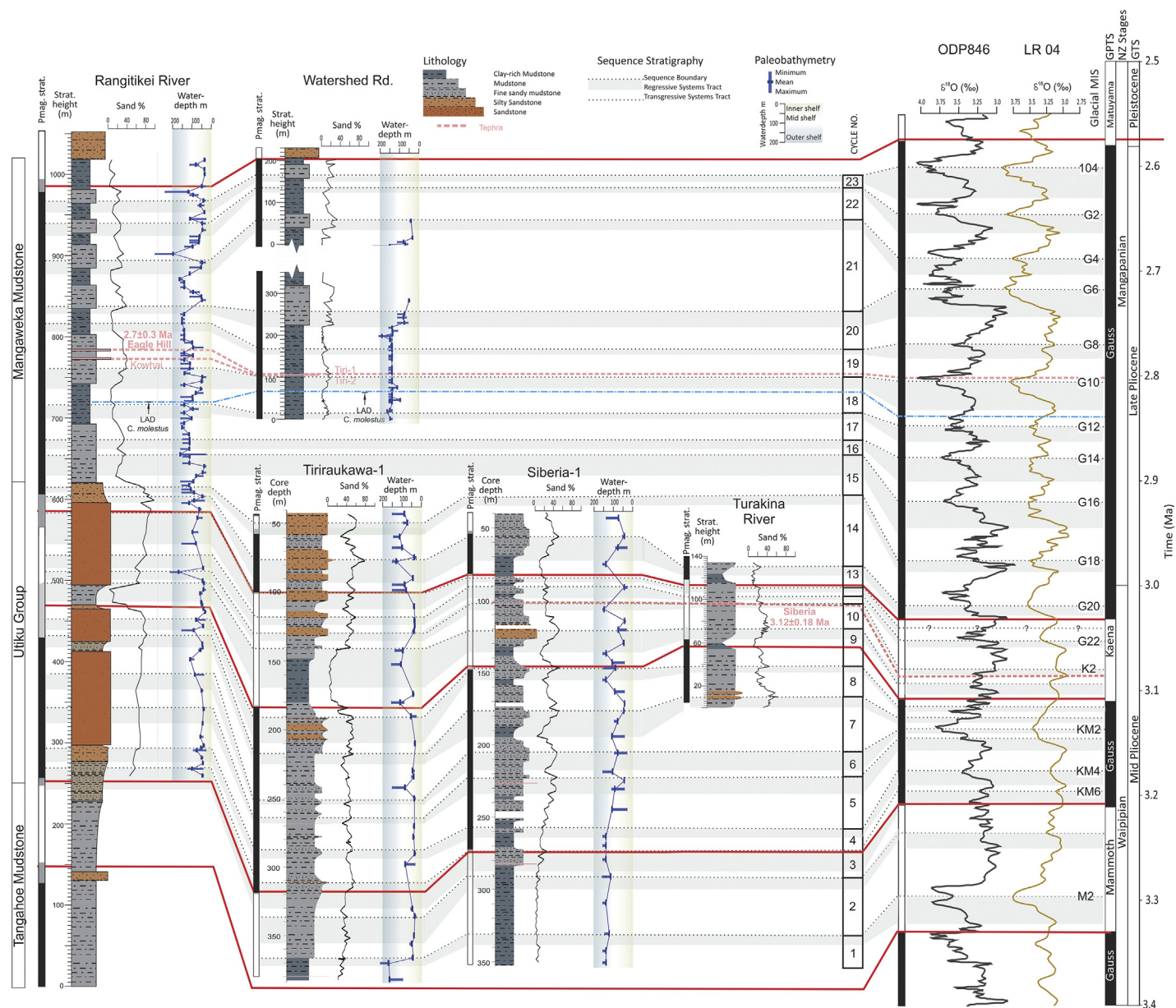


Fig. 3. (continued).

cyclically with grain size, lithology and lithofacies variations (Fig. 3a). Elevated natural gamma-radiation (NGR) activity associated with increased uranium, potassium and thorium in clay-rich sediments typically correspond to fine-grained lithologies.

Likewise, magnetic susceptibility is stronger in finer-grained sediments containing a higher proportion of sub-micron ferromagnetic grains in the superparamagnetic state (Hunt et al., 1995). Sandier sediments in the core are characterised by relatively high resistivity



**Fig. 4.** Correlation of sedimentary cycles independently-constrained by paleomagnetostratigraphy (pmag. strat.; black: normal; white: reversal; grey: uncertain) and tephra identified in outcrop sections of the Utiku Group and Mangaweka Mudstone (Rangitikei River, Watershed Road and Turakina River Sections) and drillcores (Tiriraukawa-1; Siberia-1) with published oxygen isotope records (ODP846, Shackleton et al., 1995 and LR04, Lisiecki and Raymo, 2005) and the global polarity timescale. Sand percentage provides a high resolution signature for lithofacies cycles not always identified visually by lithology, which are numbered 1 to 23. Water depths have been derived by application of the benthic foraminifera MAT. The paleomagnetic stratigraphy is after Turner et al. (2005) and Naish et al., (1996) for the Rangitikei section, Turner et al. (2005) for the Turakina section and Tapia et al., 2018, (in review) for the drill cores. Biostratigraphic datums are after Cooper et al. (2004) and Raine et al. (2015). Tephra correlation and numeric ages discussed in the text are shown. This integrated chronostratigraphic framework allows correlation of Whanganui cycles 1–23 with the high-resolution, deep sea benthic  $\delta^{18}\text{O}$  record of ODP Site 846 (Shackleton et al., 1995; using the age model provided by Lisiecki and Raymo, 2005) and the benthic  $\delta^{18}\text{O}$  stack (LR04; Lisiecki and Raymo, 2005).



and density, and low magnetic susceptibility and NGR activity.

### 3.2. Tiriraukawa-1 drillcore

Tiriraukawa-1 was spudded in August 2014, at Watershed Road, near Tiriraukawa approximately 18 km southeast of Siberia-1 and roughly halfway between the Rangitikei and Turakina rivers (S39.7625° E175.6689°; Fig. 1). It was cored continuously to a depth of 384 m with the exception of the upper 43 m, which also contained poorly-recovered unconsolidated recent colluvium. The recovered stratigraphic record contains 14 full sedimentary cycles, ranging from 10 to 60 m in thickness, within the Utiku Group spanning the downhole interval between 43 and 376 m. The cycles are generally sandier than Siberia-1 reflecting a more shoreline-proximal location, and are characterised by oscillations in grain-size from 20 to 80% sand, and lithologic changes ranging from clay-rich mudstone/mudstone to fine-sandy mudstone/muddy sandstone/sandstone (Fig. 3b). Cycle boundaries are all conformable and correspond to the inferred shallowest points as expressed by maximum sand percentage. Physical properties logs of the bore hole and the core also co-vary cyclically with grainsize, lithology and lithofacies variations (Fig. 3b) and display a similar relationship to that described for the Siberia-1 core.

### 3.3. Rangitikei river section

Rangitikei River Section in eastern Whanganui Basin contains a well-exposed 750 m thick Pliocene sedimentary succession that accumulated between 3.3 and 2.6 Ma (Journeaux et al., 1996, Fig. 1). Lithofacies analysis, including laboratory grain-size determinations, and benthic foraminiferal paleowater depth estimates show that the lower 350 m (Utiku Group) accumulated predominantly in a shoreface to inner shelf environment. The overlying 400 m-thick Mangaweka Mudstone accumulated in a middle to outer shelf environment (Kamp et al., 1998). Combined with the identification of sequence stratigraphic boundaries, 14 sedimentary cycles were identified in the Utiku Group. In the outwardly structureless Mangaweka Mudstone, 9 sedimentary cycles are defined by changes in grain size, lithofacies and foraminiferal faunas (Fig. 4; Journeaux et al., 1996). Rapid deepening of greater than 100 m across the Utiku Group–Mangaweka Mudstone boundary at ca. 3 Ma occurs within a 30 m-thick stratigraphic interval.

### 3.4. Watershed road section

Late Pliocene Mangaweka Mudstone is exposed in a semi-continuous 672 m-thick road section south of Tiriraukawa, on the

Watershed Road between the Rangitikei and Turakina River valleys (Fig. 1). A recent study by Sefton (2015) using lithofacies and benthic foraminiferal paleoecology shows that the section is dominated by clay-rich mudstone and mudstone, with 10–30% sand, deposited in outer shelf to upper slope water depths (Fig. 4). A silty sandstone lithology occurs at the top of the section near the boundary with the overlying Rangitikei Group (Naish and Kamp, 1995). While not continuously exposed, 7 cycles of grainsize and benthic foraminiferal depth assemblages have been identified.

### 3.5. Turakina river section

We present a new detailed middle Utiku Group stratigraphy based on river valley outcrop description and sedimentological analyses by Patterson (2014) at Siberia Station in the Turakina Valley south of Papanui Junction (Fig. 1; S39.69425° E175.52151°). The stratigraphy provides a higher-resolution description and grainsize measurements in the context of broad regional mapping by McGuire (1989). The ~140 m-thick composite section fines upwards from 60% to 10% sand and is dominated by 6 cyclic-alternations of clay-rich mudstone and mudstone interpreted to be deposited on the middle to outer shelf. The succession includes the Kaena reversed-geomagnetic polarity subchron and spans ~3.12–3.0 Ma (Turner et al., 2005). The stratigraphy and grain-size curve (sand percentage curve) can be readily correlated with Siberia-1 due to their close proximity and overlapping stratigraphy (Fig. 4).

## 4. Lithofacies analysis and sequence stratigraphy

The 23 cycles identified within the Utiku Group (Cycles 1–14) and the Mangaweka Mudstone (Cycles 15–23) display continuous, recurrent vertically-stacked cyclical facies successions, whose identification is augmented by continuous grain-size analyses summarised as sand percentage (Fig. 4). Each sequence or sedimentary cycle is bounded by conformable boundaries (correlative conformities: CC) marking the shallowest point as shown by sand percentage. However, erosional unconformities mark some sequence boundaries in the shallow water Utiku Group facies cycles described in the Rangitikei River Section (e.g. Fig. 4; Kamp et al., 1998). Five lithofacies, identified on the basis of lithology, bioturbation and sedimentary structures, and their interpreted depositional environments, are used to highlight cyclicity (Table 1). The vertical occurrence of the facies in each of the 23 sedimentary cycles is shown in Fig. 4. Later in this paper we provide a high-resolution age model that allows individual sedimentary cycles to be mapped from the shallow eastern margin (Rangitikei River Section) across the basin to the deeper water Turakina River

**Table 1**  
Lithofacies codes, names, description, lithology and depositional environments observed in the cores (Facies 1–4) and Facies 5 –described in outcrop by Journeaux et al. (1996). This facies scheme was also applied to the Mangaweka Group outcrop sections (described by Journeaux et al., 1996; Sefton, 2015).

Code	Facies	Description	Lithology	Depositional Environment
5	Well sorted Sandstone	Fine Sandstone, brown, moderately to highly bioturbated, sparsely fossiliferous, massive to crudely bedded m-scale.	Fine Sandstone	Shoreface to Inner shelf
4	Silty Sandstone	Silty-Sandstone, green grey to grey brown, moderately bioturbated, burrowed. Sparsely to moderately fossiliferous, cm-scale bivalve fragments <15 mm and dm-scale disarticulate and articulate bivalves up to 40 mm. Common discontinuous mm-scale lenticular laminae and sand-silt cm-scale lenses.	Silty Sandstone	Inner shelf
3	Fine sandy Mudstone	Sandy Mudstone, green-grey, firm, moderately to highly bioturbated, discontinuous mm-scale very fine sand laminae, cm-scale bivalve fragments <15 mm	Fine Sandy Mudstone	Middle shelf
2	Weakly Stratified Mudstone	Sandy- Siltstone, grey-brown, firm, moderately bioturbated and occasional burrows. Moderately fossiliferous, bivalve fragments <5 mm on mm to cm-scale. Weakly stratified with mm-scale silt horizontal lenses.	Very fine sandy Mudstone	Outer to middle shelf
1	Massive Mudstone	Clay-rich Siltstone, blue grey, firm, moderately to highly bioturbated, chondrites, rare wispy silt-sand lenses. Sparsely fossiliferous, dm-scale frequency of disarticulate bivalves and gastropoda.	Clay-rich Mudstone	Outer shelf



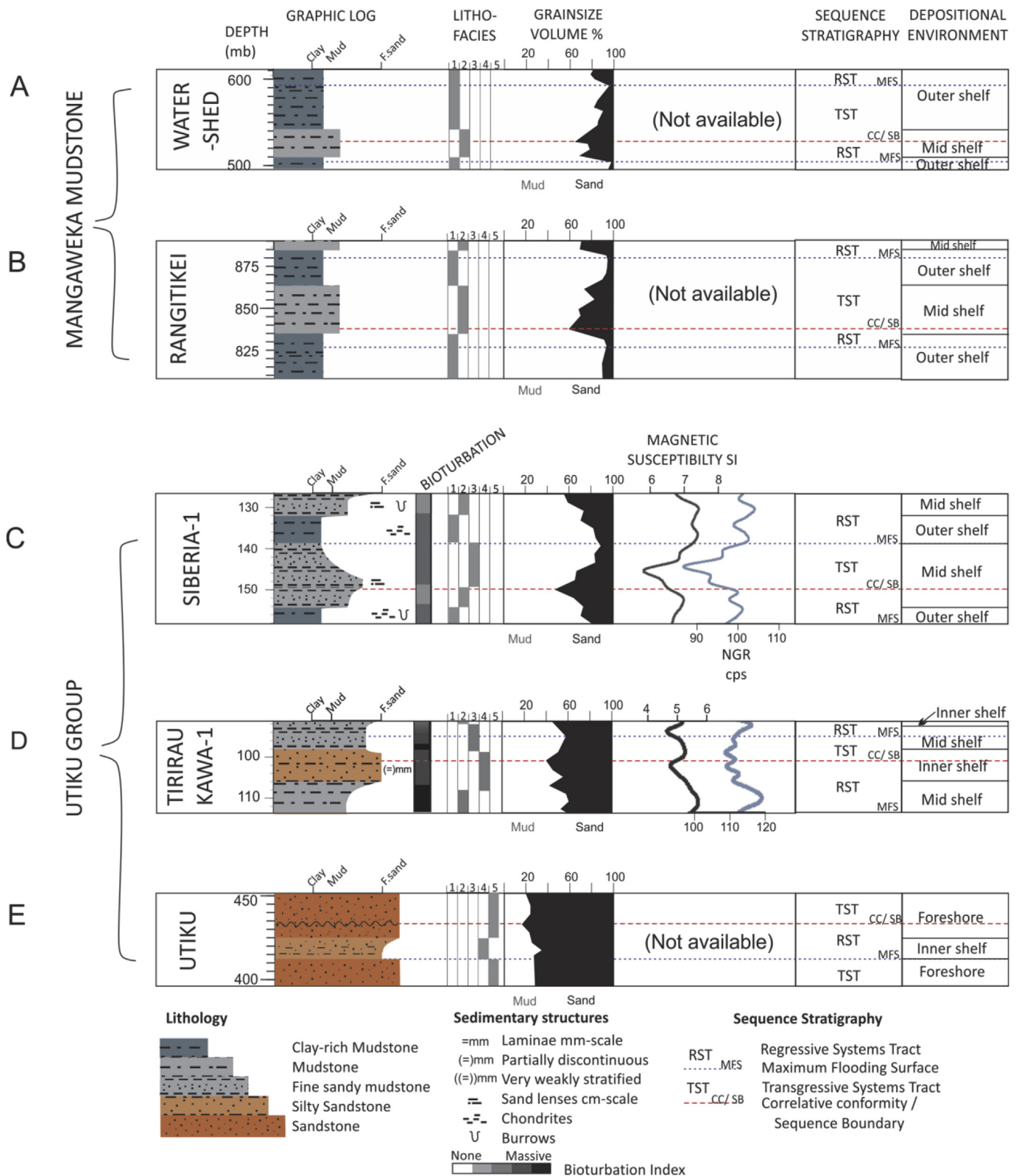


**Fig. 5.** Conceptual model developed chiefly from lithofacies and sequence stratigraphic analysis of the mid-to late Pliocene outcrop sections and drillcore illustrated in Fig. 4. Five representative sedimentary motifs (A: Watershed; B: Rangitikei; C: Siberia-1; D: Tiriraukawa-1; E: Utiku), named after the sections from which they have been synthesised, show the inferred stratigraphic position of sequence boundaries and intervening flooding surface. This helps infer transgression and regression in a cycle of relative sea-level change.

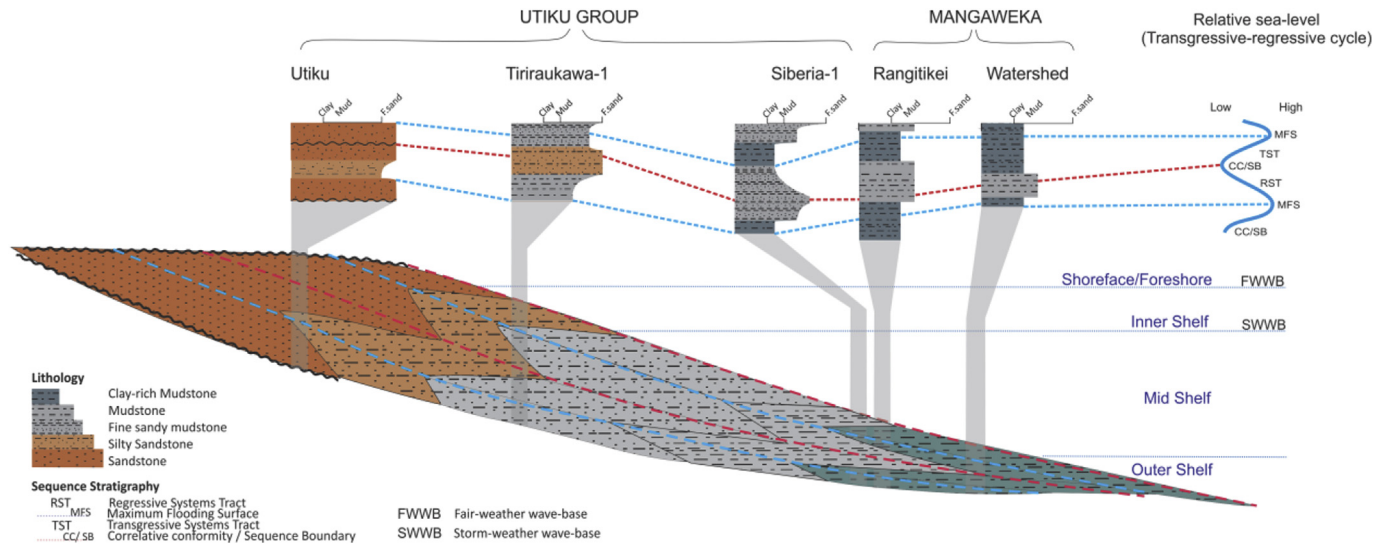


**Fig. 6.** Figure showing five sedimentary motifs (Fig. 5) arranged at increasing water depth across a shore-normal shelf cross-section to characterise the changes in lithofacies character and relative height of sequence stratigraphic surfaces in a typical mid-to late Pliocene Whanganui Basin sedimentary record of a sea-level cycle in the Utiku Group and Mangaweka Mudstone. Note how the sequence surfaces correspond to the relative sea-level cycle shown on the right.

Section/Siberia-1 drillcore further west, and correlated with orbital scale, glacial-interglacial cycles in the benthic oxygen isotope curve (Fig. 4).

We have developed a sequence stratigraphic model (Fig. 5) based on the identification of fining- (deepening) upwards facies successions assigned to the transgressive systems tract (TST), and coarsening- (shallowing) upwards facies successions assigned to the regressive systems tract (RST; e.g. Naish and Kamp, 1997a). Given the lack of erosional unconformities and the relatively low amplitude of sea-level change implied by our data, our sequence model has similarities to the two-systems tract, transgressive-regressive model of Embry (1993). The boundary between the TST and RST is the maximum flooding surface (MFS) and marks the deepest part of each cycle corresponding to minimum percentage sand. The sequence boundary is defined by the maximum sand percentage, and corresponds to the deep-water correlative conformity coincident with relative sea-level lowstand, similar to a surface of maximum regression (Embry, 1993). We have identified five characteristic sequence motifs (Fig. 5) representing deposition on different parts of a shoreline to outer shelf continuum, during a cycle of relative sea-level change (Figs. 5 and 6). While we acknowledge they are laterally-grading variants along a depositional transect, these motifs are distinguished on the basis of the regular vertical recurrence. Our interpretation of water depth is based on both sedimentological and benthic foraminiferal indicators, described in more detail below. The model substitutes time for space based on cycle correlations and time-depth relationships shown in Fig. 4. The idealised sequence architecture therefore results from a combination of descriptive facies analysis and the overlying chronostratigraphic template provided by the correlation of distinctive surfaces (sequence boundaries and maximum flooding surfaces, defined by sediment grain size) within the constraints of our age model. In the following section, the characteristics of each sequence motif are described from shallowest to deepest.

#### 4.1. Utiku motif

Utiku motifs occur in the Utiku Group exposed in the Rangitikei River Section (Fig. 5e). They are up to 60 m-thick and contain the

shallowest facies alternating between shoreface sandstone (Facies 5) and inner shelf silty sandstone (Facies 4). In some cases the lower boundary of the TST is unconformable and interpreted as erosion during subaerial exposure at sea-level lowstands and subsequent shoreline transgression (e.g. Kamp et al., 1998; Saul et al., 1999).

#### 4.2. Tiriraukawa-1 motif

Tiriraukawa cycles typically occur in the Utiku Group in the Tiriraukawa-1 drillcore (Fig. 5d). They are up to 50 m-thick and display alternations between inner shelf silty-sandstone (Facies 4) and middle shelf fine sandy-mudstone (Facies 3). They are laterally equivalent to Utiku cycles and bounded by correlative conformities (no lowstand erosion). Both magnetic susceptibility and NGR logs are markedly cyclic with finer grained clay-rich facies displaying higher values compared to clay-poor sandy facies.

#### 4.3. Siberia-1 motif

Siberia cycles typically occur in the Utiku Group in the Siberia-1 drillcore (Fig. 5c). They are up to 20 m thick and display alternations between fine sandy-mudstone and mudstone (Facies 3/2) deposited on the middle shelf and clay-rich mudstone (Facies 1) deposited on the outer shelf. They are laterally equivalent to Utiku and Tiriraukawa cycles and are bounded by correlative conformities (no lowstand erosion) further out on the shelf. Both magnetic susceptibility and NGR logs are markedly cyclic.

#### 4.4. Rangitikei and Watershed motifs

Rangitikei cycles are exposed in outcropping Mangaweka Mudstone in the Rangitikei River Section (Fig. 5b). Finer-grained, marginally deeper-water laterally-equivalent Watershed cycles are exposed in outcrop on the Watershed Road south of Tiriraukawa (Fig. 5a). Both sets of cycles are up to 60 m-thick and display alternations between middle shelf mudstone (Facies 2) and outer shelf clay-rich mudstone (Facies 1). While younger than the Utiku, Tiriraukawa and Siberia cycles, Rangitikei and Watershed cycles represent the deepest water sedimentary cycles in our model. They are generally thicker than the other inner to middle

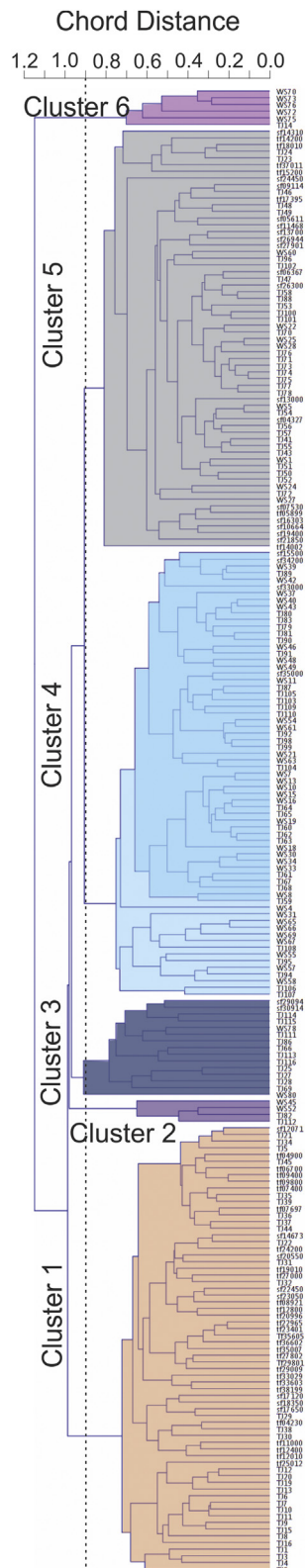


**Fig. 7.** Dendrogram classification of the 221 samples referred to in the text, for which six clusters are identified. Samples denoted TJ are for the Rangitikei River Section (Journeaux et al., 1996), WS apply to the Mangaweka Mudstone samples at the Watershed Road location (Sefton, 2015) and Tf (Tiriraukawa-1) or Sf (Siberia-1) samples were specifically collected for this investigation.

shelf cycle motifs, reflecting higher sedimentation rates during accumulation of the Mangaweka Mudstone, or a longer cycle duration.

## 5. Reconstruction of paleoenvironment, water depth & climate

The relative abundance of benthic foraminifera species preserved in marine sediments provides an environmental proxy sensitive to changes in wave and current energy, light penetration in the euphotic zone, bottom oxygenation and food availability. These environmental variables are often a function of water depth (e.g. Hayward, 1986; Hayward et al., 1999). Extant benthic foraminifera can be used to reconstruct broad changes in paleoecology, and thus determine water depth ranges. Cluster analysis of extant benthic foraminiferal faunas from the New Zealand continental shelf and shoreline, based on the relative abundance of species, has enabled the recognition of characteristic faunal associations with depositional environments (summarised in Hayward et al., 1999; Naish and Kamp, 1997b; Kamp et al., 1998; Naish and Wilson, 2009). A statistical comparison of the presence and relative abundance of extant foraminifera in the Whanganui Basin Plio-Pleistocene sediments to modern sediments (MAT; Hayward and Triggs, 2016), has allowed a more quantitative reconstruction of water depth changes.

### 5.1. Depositional environments from extant benthic foraminiferal associations

Samples selected for census counts were split before dry sieving at 150  $\mu$ m (Rangitikei and Watershed sections) and 125  $\mu$ m (drill cores), from which a minimum of 200 specimens were counted and identified at species level. We have grouped these counts at genus level because of evolutionary changes and ambiguities with nomenclature. This allows comparison of our drillcore census data with those from the Rangitikei section (Journeaux, 1995; Journeaux et al., 1996; Kamp et al., 1998) and the Watershed Road Section (Sefton, 2015) which use a different species terminology.

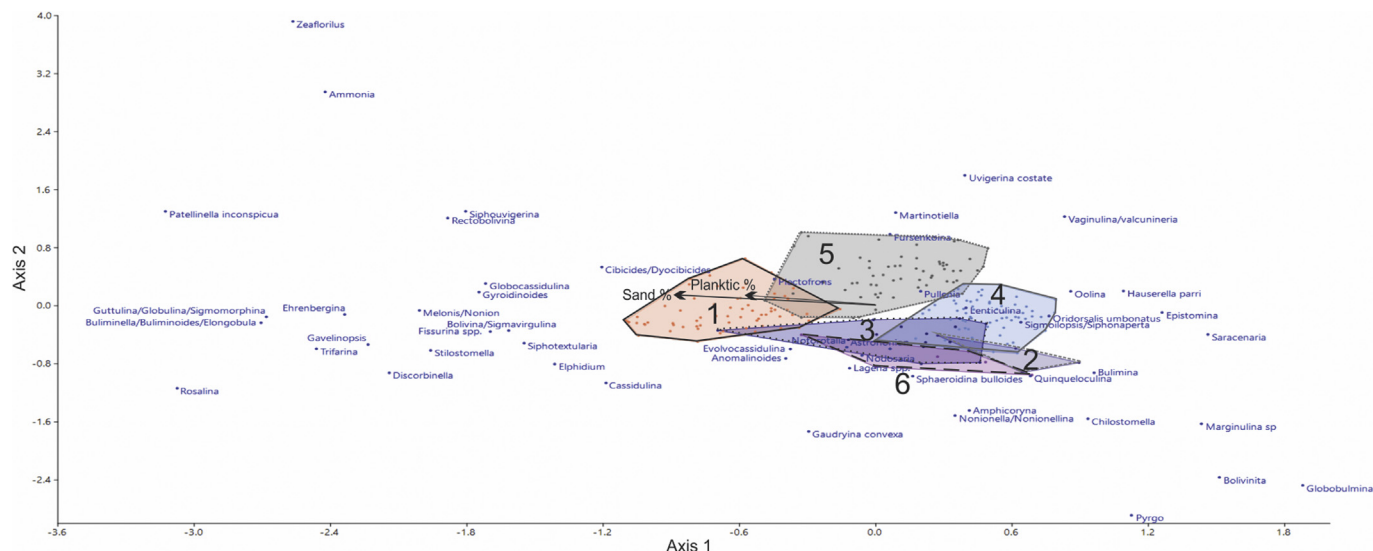
Q-mode cluster analysis using PAleontological STatistics software (PAST; Hammer et al., 2001) was undertaken on 221 samples, from the two drill cores (65 samples) and outcrops in the Rangitikei (104 samples; Kamp et al., 1998) and Watershed Road sections (47 samples; Sefton, 2015). PAST uses an unweighted, pair group average algorithm where clusters are joined on the basis of the chord distance between normalised vectors to produce a dendrogram from which associations were selected (Fig. 7). Six broad clusters were recognised, differentiated by a threshold of 0.9 on the chord distance scale, where branching occurs. Following Hayward and Triggs (2016), our chord distance was chosen to reduce the importance of highly abundant depth-insensitive (eurybathyal) genera (Hammer et al., 2001), such as *Uvigerina*, that while extant are not present in such large relative abundances today (Hayward et al., 1999). In Table 2, we list abundant extant genera (>5%) in each cluster, calculated after removing extinct genera.

While benthic foraminifera that favour shallow marine environments (<100 m) are typically viewed as more sensitive to changes in water depth than deep marine species, the minimum range of water depths inhabited by the majority of species is on the order of 50 m, which can lead to significant overlap of interpreted environments (Fig. 4.6; Hayward et al., 1999). Most studies using paleoenvironmental information derived from foraminiferal assemblages have assessed changes of large-scale water depths on the shelf representing discrete environments (~50–150 m; e.g. Naish and Kamp, 1997b; Hayward and Triggs, 2016). Foraminiferal assemblages previously recognised could not be discriminated

**Table 2**

Extant genus abundant over 10% and 5% (in brackets) for the six clusters identified in Fig. 7 with interpreted depositional environments.

	Genus >10% and (5%) abundance	Depositional environment
Cluster 1	<i>Anomalinoidea</i> , <i>Uvigerina</i> , <i>Astrononion</i> , ( <i>Elphidium</i> )	Inner to middle shelf
Cluster 2	<i>Anomalinoidea</i> , <i>Uvigerina</i> , <i>Bulimina</i> , <i>Cibicides</i> , ( <i>Notorotalia</i> , <i>Lenticulina</i> )	Outer shelf
Cluster 3	<i>Notorotalia</i> , <i>Uvigerina</i> , <i>Astrononion</i> , ( <i>Elphidium</i> )	Mainly middle shelf, extending to inner shelf
Cluster 4	<i>Uvigerina</i> , <i>Notorotalia</i> , <i>Astrononion</i> , <i>Epistomina</i> , ( <i>Anomalinoidea</i> , <i>Bulimina</i> , <i>Cibicides</i> )	Mainly middle shelf, extending to inner shelf
Cluster 5	<i>Uvigerina</i> , <i>Cibicides</i> , ( <i>Notorotalia</i> , <i>Astrononion</i> , <i>Anomalinoidea</i> )	Mainly middle shelf, extending to inner shelf
Cluster 6	<i>Bulimina</i> , <i>Notorotalia</i> , <i>Cassidulina</i> , ( <i>Astrononion</i> , <i>Uvigerina</i> , <i>Nonionellina</i> )	Outer shelf

**Fig. 8.** Two-dimensional Canonical Correspondence Analysis (PAST; Hammer et al., 2001) of Pliocene foraminiferal census data, with the genus, six clusters (identified in Fig. 7) and vector arrows of the proxy environmental factors: sand and planktic foraminiferal percentage, for the two primary axes.

conclusively on the basis of assemblages identified in this study, as most genera were common to many samples (Table 2).

However, Canonical Correspondence Analysis (CCA; Fig. 8) clearly displays a correlation between the faunal pattern, represented by the clusters/associations and percentage sand (lithology), interpreted as reflecting water depth on a wave-graded shelf, as the percentage sand vector is aligned with the first (x) axis, accounting for 62% of the variability. Known deep-water taxa such as *Epistomina elegans* (previously *Hoeglundina elegans*), *Sphaeroidina bulloides* and *Hauslerella parri* are positioned at the opposite end of the x-axis to genera of shallow-water affinity such as *Zeafloerius*, *Elphidium* and *Ammonia*, consistent with the x-axis representing changes in water depth (Fig. 8). The sand percentage vector supports the general observation that changes in grain size and benthic foraminiferal associations, and therefore sedimentary facies, reflect changes in water depth. The planktic percentage vector (Fig. 8) is commonly used as an oceanicity index (higher planktic percentage is associated with deeper waters; Hayward and Triggs, 2016), however we observe an opposite relationship in this dataset, suggesting that this relationship is less defined when only assessing shallow-marine environments.

While systematic up-core and up-section cycles in clusters do occur and broad water depth ranges can be interpreted from the depositional environments, deepening and shallowing cycles were not readily identifiable using this approach, which is relatively insensitive as a quantitative method for identifying small changes in water depth (<50 m) at shelf depths, in this study.

Based on the clusters and CCA, Cluster 1 represents the shallowest environment of the inner to middle shelf. Clusters 2 and 6, suggest relatively deeper outer shelf environment, and Clusters 3, 4

and 5 suggest middle shelf depth ranges, extending into the inner shelf. We conclude from the census data and cluster analysis that the sediments were mainly deposited within a broad inner to outer shelf depositional setting and the cluster analysis does not systematically distinguish between inner to middle or middle to outer shelf environments.

## 5.2. Depth estimates from extant benthic foraminiferal

MAT (Hayward and Triggs, 2016) was applied to the census counts of extant benthic foraminiferal genera in the core and

**Table 3**

Genus used in MAT determined by a significant correlation distance ( $1-r$  of Pearson's  $r$ ; Hammer et al., 2001) of more than  $\pm 0.3$  where 1 is a total positive correlation and  $-1$  is a total negative correlation. Bold genus were excluded for reasons outlined in the text.

	Correlation
<i>Cibicides/Dyocibicides</i>	0.732
<i>Elphidium</i>	0.700
<i>Epistomina</i>	−0.659
<i>Gavelinopsis</i>	0.5316
<i>Ehrenbergina</i>	0.479
<i>Zeafloerius</i>	0.377
<i>Nonionella/Nonionellina</i>	0.367
<i>Cassidulina</i>	0.359
<i>Gyroidinoides</i>	0.354
<i>Sphaeroidina</i>	−0.351
<i>Trifarina</i>	0.319
<b><i>Uvigerina</i></b>	<b>−0.485</b>
<b><i>Quinqueloculina</i></b>	<b>−0.452</b>



outcrop samples. This utilised a database of 240 samples of the available 626 samples (<300 m water depth) from estuarine to deep marine environments around New Zealand (Hayward et al., 1987; Hayward et al., 1999; Hayward and Triggs, 2016). The MAT determines the squared chord correlation coefficient between the Pliocene samples and modern database with known water depths (Hayward and Triggs, 2016). The taxa selected for statistical comparison, were reduced from the 38 to 11 extant genera, using only those that showed a significant positive or negative correlation (>0.3) with sand percentage considered as most depth sensitive (Table 3). *Uvigerina* was excluded due to the anomalously high counts, which are unprecedented in modern waters, leading to overestimated water depths in the Pliocene samples. *Quinqueloculina* was also excluded as it showed a strong negative correlation with sand percentage, whereas the modern environment shows a positive correlation.

A running weighted mean of the nearest three modern samples to the Pliocene samples (determined by the chord distance) was used, with the lowest and highest estimates used as the error in the method. Paleo-water depth estimates based on MAT from the foraminiferal census data are plotted with the graphical logs in Figs. 3 and 4 for all drillcore and outcrop stratigraphic sections and confirm a generally consistent relationship between percentage sand, facies and water depth.

The Utiku Group described at the Rangitikei and Tiriraukawa-1 sites does not display sufficient sensitivity of the foraminiferal-derived paleobathymetry to resolve individual sedimentary cycles identified by the grain size, lithofacies and sequence stratigraphy (Fig. 4). Siberia-1 appears to represent a “sweet-spot” on the paleo-continental shelf where the MAT is sensitive to glacial-interglacial fluctuations between middle and outer shelf water depths, and co-varies closely with facies and grain size cycles. This likely reflects the presence and absence of key outer shelf genera (e.g. *Epistomina*, *Elphidium*; Hayward et al., 1999).

The Mangaweka Mudstone, described in the Rangitikei and Watershed Road sections, represents a significant deepening from the Utiku Group, and as such, the Rangitikei River Section records middle and outer shelf environments, while the Watershed Road Section, westward on the shelf transect, records outer to upper slope environments (Fig. 4.5). Thus the Mangaweka Mudstone of the Rangitikei River Section and Utiku Group of the Siberia-1 core, represent similar water depth ranges.

The water depths determined by the MAT regularly display changes of ~100 m in Siberia-1, between minimum and maximum percent sand. This range of water depths is not supported by the paleoenvironmental interpretation of the lithofacies. However, they do match the phase and frequency of the shallowing and deepening cycles previously identified (Fig. 4).

### 5.3. Climate variability from terrestrial palynology from Siberia-1 drill core

Twenty-seven samples between 39.89 m and 299.99 m, with a sample resolution of approximately 10 m, from Siberia-1 were analysed for palynology, to determine the relationship between changes in terrestrial climate and the reconstructed water depth changes. Pollen and spore census counts were continued until one hundred pollen grains were counted on each slide and identified following the taxonomic groupings used in a comparable Pliocene marine study from ODP Site 1123, east of New Zealand (Mildenhall, 2003; Mildenhall et al., 2004). At ODP Site 1123, glacial-interglacial climate cycles are recorded as variations in carbonate percentage and showed a strong correlation with two glacial-interglacial climate-related pollen indices:

- Interglacial Vegetation (IGV) warm climate index: (*Podocarpidites* species + *Dacrydiumites praecupressinoides* [*Dacrydium*] + *Araucariacites australis* [*Agathis*]) / (*Parvisaccites catastus* [*Halocarpus*] + *Microalattidites paleogenicus* [*Phyllocladus*] + *Nothofagidites lachlaniae* [*Fuscospora*] + *Palaeocoprosmadites zelandiae* [*Coprosma*]).
- Glacial Vegetation (GV) a cool climate index, but with the possible bias from more easily transported bisaccate grains removed: (*Parvisaccites catastus* + *Microalattidites paleogenicus* + *Nothofagidites lachlaniae* + *Palaeocoprosmadites zelandiae*) / (total pollen- *Podocarpidites* species)

Pollen preservation was frequently poor, and assemblages were of low diversity. Spores were approximately twice as abundant as pollen and were dominated by *Cyathidites* species (*Cyathia*). Pollen assemblages were dominated by *Podocarpidites* species, with common *Dacrydiumites praecupressinoides* and *Nothofagidites lachlaniae*.

Variation in pollen assemblages were positively correlated with water depth changes inferred from the other environmental datasets, such that warm climate pollen assemblages (IGV) coincided with finer grained sediment and deeper water facies, and colder climate pollen assemblages corresponded with sandier sediments, and shallow-water facies (Fig. 3a). Although the depositional environment of the Siberia-1 core is considerably more proximal to land than ODP Site 1123, these ratios confirm climatically-driven vegetation changes were associated with our reconstructions of mid- to late Pliocene glacial-interglacial water depth variability.

The variability of palynology index values on glacial-interglacial timescales is generally less than reported for the Middle and Late Pleistocene from ODP Site 1123 (Mildenhall et al., 2004). There, IGV index values (typically 18–20 units), varied between –10 and +10. In contrast, IGV variation in the Siberia-1 core was in most cases <10 IGV units. For the GV index, the glacial-interglacial variation at ODP Site 1123 was ~50 units, again about twice as large as the glacial-interglacial in GV index values in the Siberia-1 core. This may reflect relatively muted vegetation change on glacial-interglacial scales during the mid-Pliocene (this study) compared to those driven by Pleistocene glacial-interglacial climate variability.

## 6. Chronostratigraphy

A chronostratigraphic framework for the mid-to late Pliocene sedimentary cycles is presented in Fig. 4. It allows recognition and correlation of 23 individual glacial-interglacial sedimentary cycles within drill core and outcrop data sets with individual cycles in benthic  $\delta^{18}\text{O}$  oxygen isotope record between 3.3 and 2.6 Ma. Our age model is based on the integration of previously published chronologies for the Rangitikei and Turakina River Sections (Journeaux et al., 1996; Naish et al., 1998; Kamp et al., 1998; Turner et al., 2005) with a new high-resolution magnetostratigraphy for the Siberia-1 and Tiriraukawa-1 drill cores and the Watershed Road outcrop section (Tapia et al., 2018, in review). It is constrained by biostratigraphy, numeric ages on rhyolitic tephra and their correlation to well-dated IODP Site 1124 record off eastern New Zealand (Fig. 1).

### 6.1. Tephrostratigraphy & tephrochronology

Silicic arc volcanism, associated with the evolution of subduction of the Pacific Plate under western North Island, has regularly contributed both primary and secondary silicic volcanoclastic deposits to Whanganui Basin (Naish et al., 1996, 1998; Pillans et al., 2005) over the last 5 Ma. The well-dated ODP Site 1124 core,

**Table 4**

Summary of individual glass shard major-element compositions of tephra beds from the Mangaweka Mudstone at the Watershed Road section (Tiri-1 and -2 tephra), Ruahine Road Section, Mangaweka (Eagle Hill and Kowhai tephra), and the Siberia tephra located in Utiku Group in the Turakina Valley (Sefton, 2015). M12 tephra from ODP-1124C (Stevens, 2010) are included for comparison. Data displayed are weight percent means calculated on a water-free basis. Standard deviation ( $\pm 1$  SD) is indicated in brackets below mean values. All major element determinations were made on a JEOL Superprobe (JXA-8230) housed at Victoria University of Wellington, using the ZAF correction method. Analyses were performed using an accelerating voltage of 15 kV under a static electron beam operating at 8 nA. The electron beam was defocused between 10 and 20  $\mu\text{m}$ . Analysts: B. V. Alloway and J. Sefton, #M.T. Stevens. For electron microprobe analyses of other ODP-1124C tephra of similar age (i.e. M9, M10, M13, M14 and M15; see Fig. 10) please also refer to Stevens (2010).

	Mount position probe run	SiO <sub>2</sub>	Al <sub>2</sub> O <sub>3</sub>	TiO <sub>2</sub>	FeO	MgO	MnO	CaO	Na <sub>2</sub> O	K <sub>2</sub> O	Cl	H <sub>2</sub> O	n
<b>Kowhai Tephra</b>	10-06-04 (Aug. 21, 2014)	77.77 (0.58)	12.67 (0.19)	0.10 (0.02)	1.37 (0.09)	0.08 (0.06)	0.03 (0.01)	0.92 (0.10)	3.55 (0.37)	3.33 (0.19)	0.18 (0.01)	3.91 (0.92)	20
<b>Tiri-1 tephra</b>	14-J1-4 (Aug. 21, 2014)	76.42 (0.90)	12.60 (0.12)	0.09 (0.02)	1.34 (0.06)	0.08 (0.06)	0.03 (0.02)	0.88 (0.02)	4.51 (0.74)	3.87 (0.27)	0.18 (0.01)	4.83 (1.23)	19
<b>Eagle Hill Tephra</b>	10-06-03 (Aug. 21, 2014)	74.74 (0.53)	14.20 (0.12)	0.40 (0.02)	2.84 (0.11)	0.37 (0.07)	0.05 (0.01)	2.24 (0.07)	2.57 (0.69)	2.42 (0.20)	0.15 (0.02)	6.68 (1.66)	17
<b>Tiri-2 tephra</b>	14-J1-5 (Aug. 21, 2014)	74.22 (0.41)	14.26 (0.13)	0.41 (0.01)	2.78 (0.08)	0.40 (0.07)	0.06 (0.02)	2.24 (0.10)	2.93 (0.43)	2.54 (0.11)	0.16 (0.01)	6.55 (1.02)	20
<b>Siberia tephra</b>	10-06-01 (Aug. 21, 2014)	76.06 (0.54)	12.94 (0.22)	0.19 (0.02)	1.42 (0.12)	0.20 (0.06)	0.04 (0.10)	1.33 (0.10)	4.47 (0.52)	3.16 (0.13)	0.19 (0.01)	3.68 (1.03)	18
<b>M12 (upper) <sup>#</sup> - formerly M11 1124C-9H-2W-145 (mbsf 87.10 m)</b>		77.00 (1.77)	12.70 (0.88)	0.21 (0.11)	1.40 (0.38)	0.21 (0.12)	—	1.40 (0.38)	3.50 (0.47)	3.44 (0.45)	0.18 (0.09)	4.71 (2.51)	18
<b>M12 (lower) <sup>#</sup> 1124C-9H-3W-20 (mbsf 87.40 m) — 3.090 Ma</b>		76.10 (1.72)	13.30 (1.03)	0.18 (0.12)	1.43 (0.50)	0.23 (0.14)	—	1.37 (0.48)	3.84 (0.32)	3.38 (0.69)	0.19 (0.07)	5.45 (1.36)	18
<b>Glass Standard ATHO-G</b>	(Aug. 21, 2014)	75.61 (0.54)	12.20 (0.09)	0.26 (0.02)	3.27 (0.11)	0.10 (0.06)	0.11 (0.02)	1.70 (0.05)	3.73 (0.28)	2.64 (0.05)	0.05 (0.03)	99.66 (0.76)	73

located east of New Zealand and downwind from onshore eruptive centres (Fig. 1), preserves a detailed eruption history of distal airfall deposits from both the Coromandel and Taupo volcanic centres over the last 10–2 Ma and <2 Ma years, respectively (Carter et al., 2003, 2004). Many of these ODP Site 1124 tephra have been geochemically characterised using glass shard major and trace element chemistry, and correlated to equivalent-aged tephra preserved within Whanganui Basin (e.g. Alloway et al., 2004, 2005).

#### 6.1.1. Siberia Tephra

An ~40 cm-thick, laterally-discontinuous, white-grey vitric-rich lapilli and ash bed, outcrops within fine-sandy mudstone of the Utiku Group in the Turakina River Section (McGuire, 1989; Patterson, 2014), and occurs stratigraphically within Kaena Subchron (33 m above the base; Fig. 4; Turner et al., 2005). Its type section is located on the true right bank of the river (S 39.69576° E 175.52099°) near a farm track bridge. Its base is marked by a sharp and wavy erosional lower contact with mudstone containing fine to medium pumiceous lapilli, grading upwards to fine vitric sand and silt that typically exhibit cm-thick parallel and planar cross-stratification. Increased bioturbation towards the upper gradational contact is indicated by distinctive 10 cm-long burrows backfilled with marine mudstone.

Siberia Tephra resembles a shelf turbidite occurring within fine sandy-mudstone (Facies 3) at its type locality. Based on both the sedimentological architecture of this unit together with glass-shard geochemistry, which indicates a homogeneous composition (see below), we interpret this deposit as a submarine non-cohesive mass flow that likely originated as remobilised silicic volcanoclastic material that was channelised in the aftermath of a large onshore eruption and then transported offshore. Presently it is unknown if the Siberia Tephra at this occurrence represents the distal end-member of a proximal gas- (i.e. pyroclastic flow) to distal water- (i.e. hyperconcentrated-to flood-flow) supported continuum.

While this channelised tephra was not identified in the Siberia-1 drillcore, located only 300 m to the east of the type locality, its stratigraphic position was established on the basis of the similarity of grain size curves, which allows accurate correlation of the sedimentary cycles described in outcrop with the drill core (Fig. 4).

Major and trace element compositions of individual glass shards from both the Siberia tephra, at its type locality, and potential correlatives in the ODP Site 1124C core were characterised using electron microprobe and Laser Ablation-Inductively coupled plasma mass spectrometry (LA-ICP-MS) techniques (Tables 4 and 5). Selected major element bivariate plots (Fig. 9) and a similarity coefficient of >0.92 establishes a strong correlation between Siberia Tephra and an equivalent-aged tephra (M12-upper and M12-lower; see Fig. 9) occurring within a paleomagnetic interval of ODP Site 1124C identified as the Kaena subchron (3.116–3.032). ODP Site 1124 tephra beds have been dated by linear interpolation of sedimentation rates between astronomically-tuned key paleomagnetic polarity boundaries (Carter et al., 2003, 2004; Stevens, 2010). Consequently, the base of M12 tephra has an estimated age of 3.090 Ma. Originally, the M12-upper (this study) was previously named M11 (Stevens, 2010) and occurred at the base of core section 1124C-9H-2W-145 at mbsf 87.10 m. However, this tephra layer is now recognised as a continuation of M12 occurring within the uppermost part of the immediately underlying core section (1124C-9H-3W-20 at mbsf 87.40 m), and therefore, is regarded in this study as a discrete layer representing the same eruptive event. Correlation between Siberia tephra and M12 is further supported by selected trace element bivariate plots (i.e. Sr v's Nd, Zr, Zr v's Nd, Y and Nd v's Th; Fig. 10; Table 5).

An age for the Siberia Tephra of  $3.12 \pm 0.18$  Ma was established from U-Th-Pb analyses of zircon at Victoria University of Wellington, New Zealand, following the methods of Sagar and Palin (2011). This age confirms the more precise stratigraphic age established on the basis of tephrostratigraphy, but more importantly constrains the magnetostratigraphic interpretation (Fig. 11).

#### 6.1.2. Tiri tephra

Two thin (<5 cm-thick), white, heavily-bioturbated and discontinuous vitric-rich tephra horizons, stratigraphically separated by 8 m of mudstone, outcrop on Watershed Road (S39.7726° E175.6755°) 150 m above the base of the Mangaweka Mudstone within clay-rich outer shelf mudstone (Facies 1). The lower and upper tephra are named Tiri-1 and Tiri-2 respectively. Glass shards from both Tiri tephra as well as two potential correlatives, Kowhai and Eagle Hill tephra previously described from sections along

**Table 5**

Summary of glass shard trace element compositions of mid-to late Pliocene tephra, Whanganui Basin, obtained by LA-ICP-MS at University of Wales, Aberystwyth, analyst: B. V. Alloway. All concentrations in ppm unless otherwise stated, standard deviation ( $\pm 1$  SD) is indicated in brackets below mean values. Trace element data from two ODP-1124C tephra (M12-upper (formerly M11) and M12-lower) obtained by LA-ICP-MS at Victoria University of Wellington by Stevens (2010) are included for direct comparison with Siberia tephra. For VUW LA-ICP-MS operational specifications and standards as well as, trace element glass shard data for similar-aged ODP-1124C tephra (i.e. M9, M10, M13, M14 and M15) please refer to Stevens (2010). Individual trace-element analyses are available upon request.

Sample	Int'l std - SiO2 wt%	Rb	Sr	Y	Zr	Nb	Cs	Ba	La	Ce
<b>Kowhai Tephra</b> (10-06-4)	77.77	152.07 (6.73)	78.49 (13.96)	37.57 (3.63)	158.15 (29.64)	9.58 (0.80)	6.24 (0.37)	1031.52 (87.76)	33.20 (3.15)	66.27 (4.22)
<b>Tiri-1 tephra</b> (14-J1-4)	76.42	152.22 (9.33)	81.74 (15.77)	37.13 (3.49)	143.23 (24.52)	8.83 (0.63)	6.27 (0.65)	1083.20 (69.14)	32.71 (4.82)	65.77 (5.26)
<b>Eagle Hill Tephra</b> (10-06-3)	74.74	117.12 (5.50)	180.22 (17.01)	38.00 (3.40)	299.82 (25.17)	9.26 (0.70)	5.24 (0.30)	852.48 (49.09)	27.91 (2.51)	55.82 (4.46)
<b>Tiri-2 tephra</b> (14-J1-5)	74.22	133.97 (20.40)	152.77 (35.73)	33.90 (2.39)	255.21 (26.27)	9.39 (0.72)	5.65 (0.53)	847.36 (61.36)	26.00 (1.93)	54.83 (2.79)
<b>Siberia Tephra</b> (10-06-1)	76.53	116.23 (12.74)	114.98 (39.11)	28.70 (4.25)	198.28 (34.68)	7.33 (0.82)	5.21 (0.87)	958.29 (113.01)	25.98 (3.35)	48.03 (5.24)
<b>ATHO-G GeoReM Accepted Values</b>	1.7	65.3 (3.00)	94.1 (2.70)	94.5 (3.50)	512 (20.00)	62.4 (2.60)	1.08 (0.11)	547 (16.00)	55.6 (1.50)	121 (4.00)
<b>ATHO-G May 2014 Analyses</b>	1.66 (0.17)	65.09 (3.45)	94.62 (5.16)	99.61 (4.72)	524.24 (28.04)	62.85 (2.29)	1.01 (0.13)	528.90 (22.56)	54.69 (2.56)	118.19 (7.80)
<b>M12-upper*</b> (formerly M11)		126.04 (5.96)	80.69 (16.34)	24.10 (7.27)	156.40 (42.71)	7.09 (0.95)	7.53 (0.58)	839.64 (53.04)	22.46 (3.86)	44.61 (3.67)
<b>M12-lower*</b>		135.15 (19.58)	89.81 (21.08)	22.93 (5.93)	172.11 (57.55)	7.25 (0.73)	8.13 (1.56)	864.83 (86.66)	22.92 (3.37)	45.36 (3.96)
Sample	Pr	Nd	Sm	Eu	Gd	Tb	Dy	Ho	Er	Tm
<b>Kowhai Tephra</b> (10-06-4)	7.30 (0.75)	29.75 (3.17)	6.74 (1.06)	0.81 (0.25)	6.62 (1.61)	1.05 (0.20)	6.72 (0.84)	1.42 (0.24)	3.99 (0.78)	0.67 (0.16)
<b>Tiri-1 tephra</b> (14-J1-4)	7.56 (0.95)	31.10 (4.47)	6.89 (1.77)	0.88 (0.30)	6.89 (1.89)	1.01 (0.18)	6.65 (1.25)	1.36 (0.28)	4.17 (0.77)	0.68 (0.38)
<b>Eagle Hill Tephra</b> (10-06-3)	6.70 (0.60)	28.54 (2.94)	6.06 (1.29)	1.11 (0.29)	6.87 (1.53)	1.02 (0.18)	6.99 (0.81)	1.41 (0.19)	4.19 (0.69)	0.60 (0.13)
<b>Tiri-2 tephra</b> (14-J1-5)	6.26 (0.47)	25.42 (3.04)	6.34 (1.67)	0.99 (0.25)	6.02 (1.45)	0.94 (0.18)	6.09 (0.88)	1.26 (0.22)	4.04 (0.61)	0.58 (0.11)
<b>Siberia Tephra</b> (10-06-1)	5.67 (0.71)	22.28 (3.30)	4.76 (1.30)	0.71 (0.31)	4.65 (1.60)	0.77 (0.16)	4.64 (0.84)	1.04 (0.24)	3.13 (1.04)	0.55 (0.20)
<b>ATHO-G GeoReM Accepted Values</b>	14.6 (0.40)	60.9 (2.00)	14.2 (0.40)	2.76 (0.10)	15.3 (0.70)	2.51 (0.08)	16.2 (0.70)	3.43 (0.11)	10.3 (0.50)	1.52 (0.07)
<b>ATHO-G May 2014 Analyses</b>	14.12 (0.73)	59.57 (4.00)	14.11 (1.30)	2.69 (0.30)	15.71 (1.36)	2.62 (0.27)	16.33 (1.18)	3.69 (0.27)	11.12 (1.19)	1.58 (0.15)
<b>M12-upper</b> (formerly M11)	4.76 (0.70)	18.93 (3.47)	2.73 (1.45)	0.43 (0.30)	3.33 (1.40)	0.45 (0.14)	3.82 (0.81)	0.80 (0.25)	2.50 (0.70)	0.33 (0.25)
<b>M12-lower</b>	4.72 (0.57)	18.32 (3.38)	3.59 (0.76)	0.60 (0.15)	3.44 (0.96)	0.52 (0.11)	3.64 (0.80)	0.78 (0.16)	2.42 (0.60)	0.37 (0.11)
Sample	Yb	Lu	Hf	Ta	Th	U	n			
<b>Kowhai Tephra</b> (10-06-4)	4.12 (0.59)	0.67 (0.18)	5.71 (0.95)	0.99 (0.19)	18.15 (1.64)	5.09 (1.87)	22			
<b>Tiri-1 tephra</b> (14-J1-4)	4.26 (1.33)	0.68 (0.26)	5.51 (1.63)	0.94 (0.24)	17.87 (2.51)	6.16 (5.74)	21			
<b>Eagle Hill Tephra</b> (10-06-3)	4.03 (0.58)	0.67 (0.16)	8.14 (0.92)	0.77 (0.20)	13.49 (0.99)	3.18 (0.43)	21			
<b>Tiri-2 tephra</b> (14-J1-5)	3.71 (0.49)	0.60 (0.16)	7.74 (0.78)	0.80 (0.20)	12.64 (1.25)	3.46 (0.46)	22			
<b>Siberia Tephra</b> (10-06-1)	3.46 (0.79)	0.62 (0.20)	6.13 (1.53)	0.75 (0.25)	15.06 (1.58)	3.39 (0.41)	25			
<b>ATHO-G GeoReM Accepted Values</b>	10.5 (0.40)	1.54 (0.05)	13.7 (0.50)	3.9 (0.20)	7.4 (0.27)	2.37 (0.12)				
<b>ATHO-G May 2014 Analyses</b>	10.59 (0.90)	1.55 (0.19)	14.13 (1.06)	4.02 (0.23)	7.31 (0.47)	2.38 (0.20)	36			
<b>M12-upper</b> (formerly M11)	2.06 (0.59)	0.38 (0.30)	3.94 (1.21)	0.53 (0.28)	12.97 (2.72)	2.53 (0.29)	13			
<b>M12-lower</b>	2.68 (0.68)	0.40 (0.09)	5.08 (1.34)	0.73 (0.12)	14.35 (3.17)	3.23 (0.55)	18			

Ruahine Road, Mangaweka (Naish et al., 1996), were geochemically characterised by electron microprobe and LA-ICP-MS techniques.

While all tephra can be classified as rhyolitic (Le Maitre, 1984), the Eagle Hill tephra and Tiri-2 are noticeably distinctive from Kowhai and Tiri-1 tephra on the basis of their glass shard major element chemistry (i.e. FeO v's CaO, K<sub>2</sub>O, TiO<sub>2</sub>; Fig. 9; Table 4). Similarly, these same tephra can be clearly distinguished by glass shard trace element concentrations (i.e. Sr v's Nd, Zr, Zr v's Nd, Y and

Nd v's Th; Fig. 10; Table 5), which confirms tephra correlation indicated from major element chemistry.

In this study, we have derived a zircon fission-track age of  $2.7 \pm 0.3$  Ma (1  $\sigma$ ; Fig. 12) for Eagle Hill Tephra (Tiri-2 correlative) at its type locality in the Rangitikei River Section (Naish et al., 1996). While the error is large, the weighted mean is statistically indistinguishable from a stratigraphic age of 2.88 Ma derived using sedimentation rates (Naish et al., 1996) and U/Pb age of

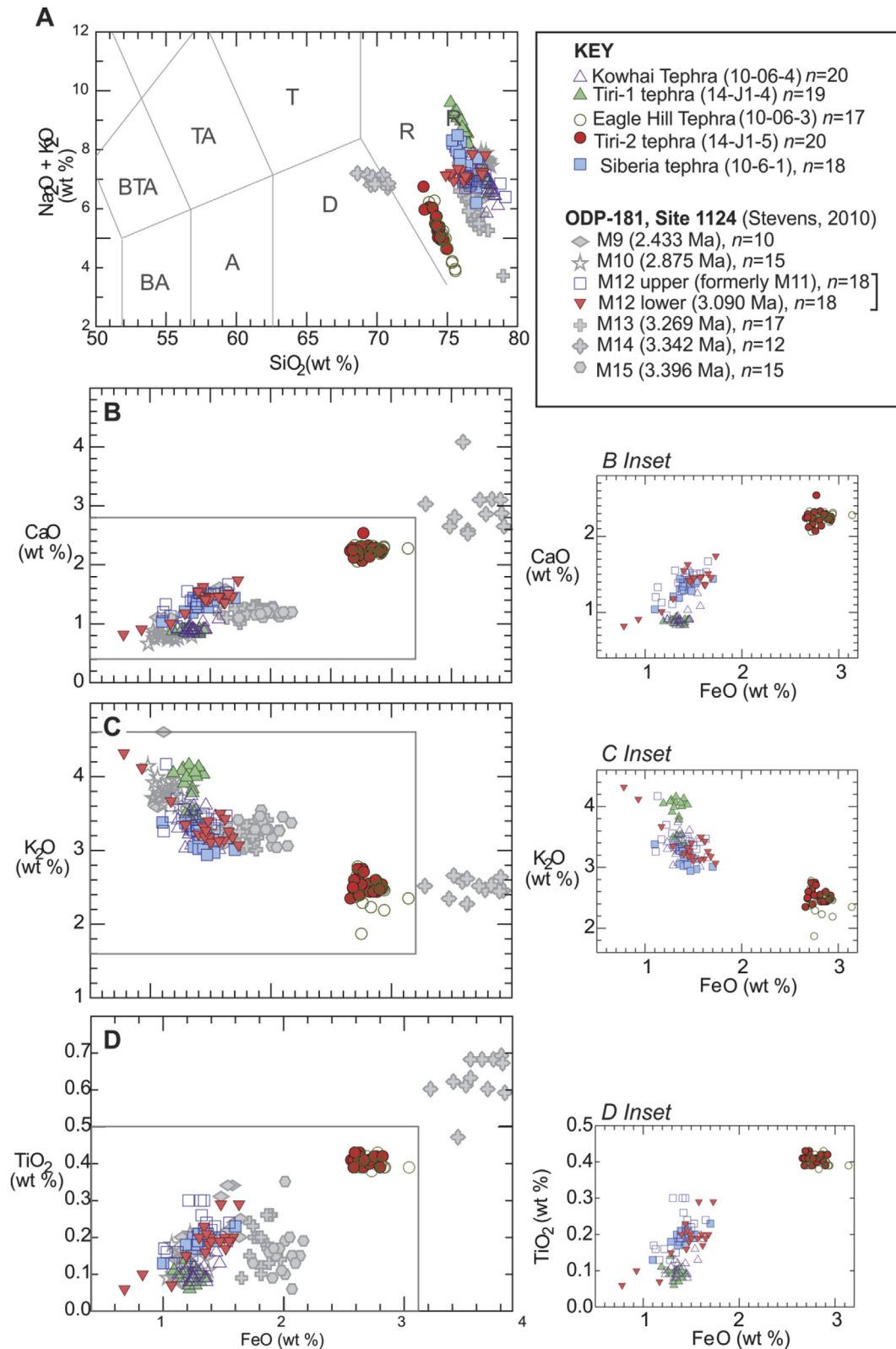


**Fig. 9.** A. Plots of SiO<sub>2</sub> vs Na<sub>2</sub>O + K<sub>2</sub>O (wt %) compositions of glass shards from mid-to late Pliocene tephra beds exposed in Whanganui Basin compared with similar aged tephra from ODP Site 1124C. All tephra are rhyolitic in composition (after [Le Maitre, 1984](#)) except for M14 (ODP Site 1124C), which straddles the rhyolite-dacite domains; **B-D**. Selected major element compositions (weight percent FeO vs CaO, K<sub>2</sub>O and TiO<sub>2</sub>) of glass shards from Kowhai, Tiri-1, Eagle Hill, Tiri-2, and Siberia tephra ([Sefton, 2015](#)) in comparison with seven tephra (M9, M10, M12 (upper; formerly M11), M12 (lower), M13, M14 and M15) of broadly similar age analysed from ODP Site 1124C ([Stevens, 2010](#)). The ODP-tephra beds have been dated by linear interpolation of sedimentation rates between astronomically-tuned key paleomagnetic polarity boundaries and ITPFT-dated tephra ([Carter et al., 2003, 2004; Alloway et al., 2005](#)). Insets highlight those tephra that are correlated in this study.



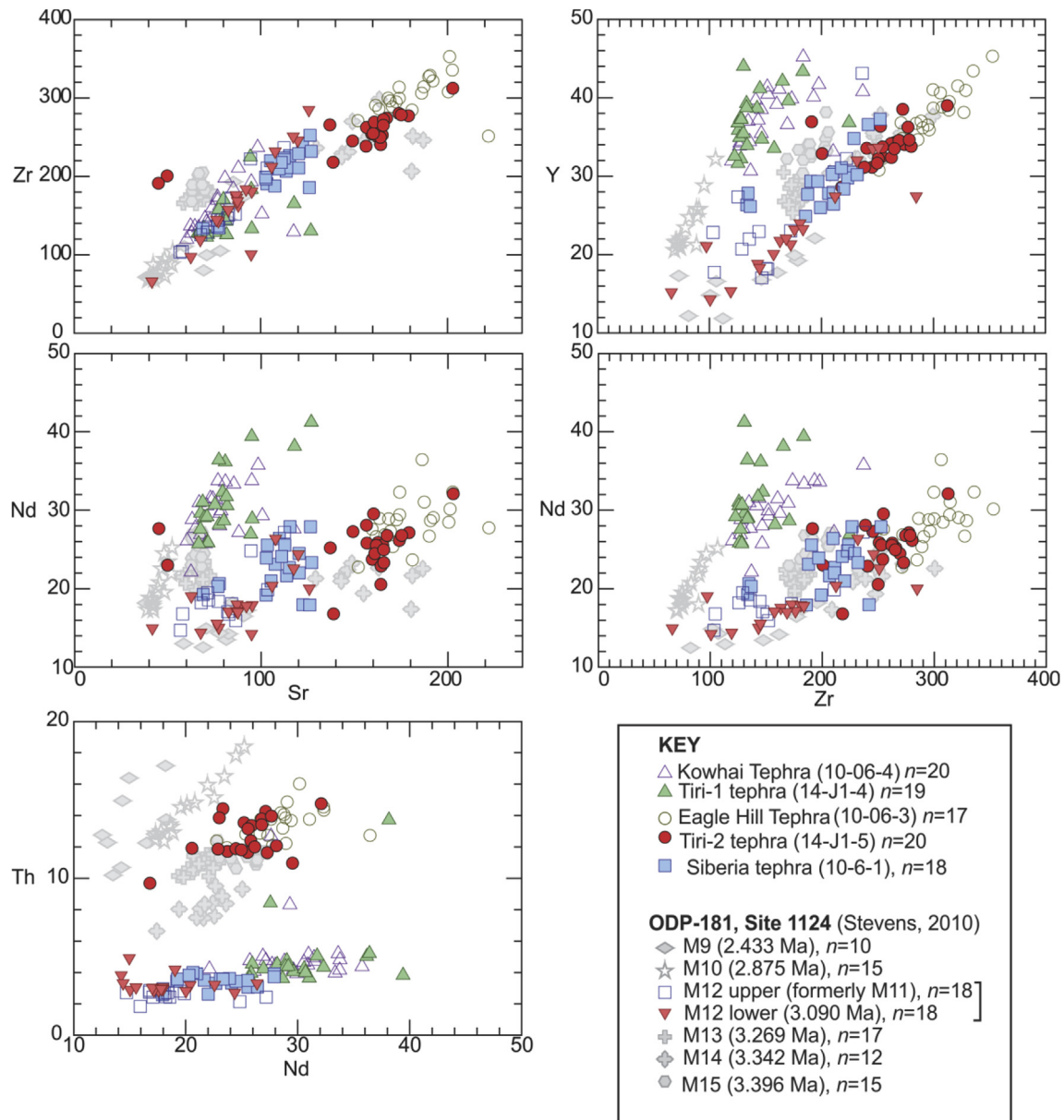


**Fig. 10.** Selected trace element bivariate plots (Sr v's Nd, Zr, Zr v's Nd, Y and Nd v's Th) determined by grain discrete LA-ICP-MS analysis (Table 5). Here, Kowhai, Tiri-1, Eagle Hill, Tiri-2 and Siberia tephra (Sefton, 2015) are plotted with respect to seven tephra (M9, M10, M12-upper, M12-lower, M13, M14 and M15) of similar age analysed from ODP Site 1124C (Stevens, 2010). Tephra symbols are the same as those listed in Fig. 9.

$2.85 \pm 0.2$  Ma reported by McIntyre (2002).

The correlation of the Eagle Hill and Kowhai to Tiri-2 and Tiri-1 tephra constrains the magnetostratigraphic interpretation of the Watershed Road section (see below), which supports the one-to-one correlation of sedimentary cycles within the Mangaweka Mudstone between the Watershed and Rangitikei sections. This correlation suggests that the Eagle Hill and Kowhai (Tiri-2 and Tiri-1) tephra were deposited between marine isotope stage G10-G9 (~2.8 Ma; Fig. 4).

## 6.2. Biostratigraphy

Key biostratigraphic constraints include:

- (i) The occurrence throughout Tiriraukawa-1 core and Rangitikei River Section of the scallop *Mesopeplum crawfordi* within

the Utiku Group, which is restricted to the New Zealand Waipian biostratigraphic stage (3.7–3.0 Ma; Beu and Maxwell, 1990; Raine et al., 2015).

- (ii) The Last Appearance Datum (LAD) of the benthic foraminifera *Cibicides molestus* toward the base of the Mangaweka Mudstone in the Rangitikei River (Journeaux et al., 1996), Watershed Road, and Turakina River Sections (McGuire, 1989) has previously been assigned to the base of the Mangapanian Stage dated to ca. 3 Ma (Cooper et al., 2004). However, this datum has been demonstrated to be diachronous across Whanganui Basin due to the restricted depositional environment of *C. molestus* (Cooper et al., 2004). A linear sedimentation rate of 0.89 m/kyr (for the first Gauss Normal subchron 3.032–2.58 Ma) dates the LAD to 2.88 Ma, while the one-to-one correlation of sequence stratigraphic cycles to the benthic  $\delta^{18}\text{O}$  record, in this study,

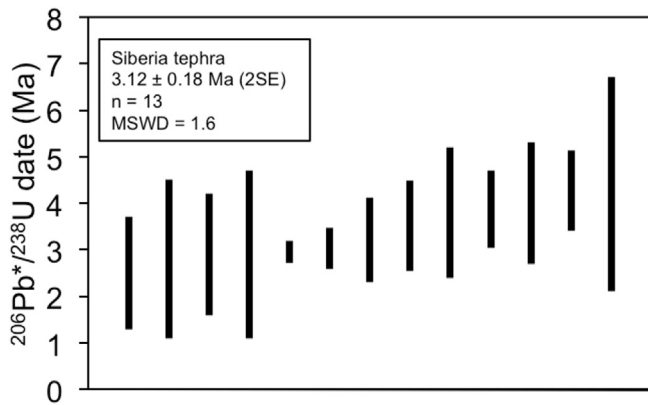


**Fig. 11.** Isoplot of 13 crystals Pb/U measurements from discrete zircons, with the weighted mean calculated at  $3.12 \pm 0.18$  Ma. U–Th–Pb–TE isotopic analyses were performed with an Australian Scientific Instruments RESOLUTION SE excimer (193 nm) laser ablation system, fitted to a Laurin Technic SR–155 sample cell and an Agilent 7500cs quadrupole inductively-coupled plasma mass spectrometer (ICP–MS). The forty analysed zircons have common-Pb corrected ( $^{206}\text{Pb}^*/^{238}\text{U}$ ) dates ranging from 2.5 to 1147 Ma, excluding those dates that are negative within error. Twenty-one of the dates are Cenozoic, 13 of which yield an error-weighted mean  $^{206}\text{Pb}^*/^{238}\text{U}$  age of  $3.12 \pm 0.18$  Ma ( $n = 13$ ; mean squared weighted deviation (MSWD) = 1.6). Dates that are clearly inherited were excluded from the error-weighted mean age calculation, along with those identified using the TuffZirc algorithm of Isoplot 4.15 (Ludwig and Mundil, 2002) as subtle inheritance, having excessive errors, or affected by minor Pb-loss.

dates the LAD between marine isotope stage G12 and G11 (~2.85–2.83 Ma).

### 6.3. Magnetostratigraphy & correlation to the geomagnetic polarity timescale (GPTS)

Metre-spaced sampling resolved a R–N–R–N–R (upward) polarity zonation for the Siberia-1 drill core and a R–N–R–N–R (upward) polarity zonation for the Tiriraukawa-1 drill core (Fig. 4; Tapia et al., 2018, in review). The R–N–R–N (upward) polarity zonation previously described for the Utiku Group strata in Rangitikei and Turakina River Sections was interpreted as the Mammoth (3.330–3.207 Ma) and Kaena (3.116–3.032 Ma) reversed polarity subchrons within the Gauss normal chron (3.580–2.581 Ma) based on their positions within much longer polarity zonations and biostratigraphic constraints (Turner et al., 2005) and the age of the younger basin-fill (Naish et al., 1998). The presence of a short reversed polarity interval in the top of both drill cores is suggested to be a previously undocumented short-lived polarity interval or cryptochron within the Gauss Normal Chron recorded because of high sedimentation rates (1–2 m/kyr) and the highly-resolved sampling (Tapia et al., 2018, in review).

It is unlikely to correspond to the Gauss/Matuyama N–R transition (2.58 Ma), as in the Rangitikei and Turakina, this occurs in the upper part of the Mangaweka Mudstone, some 400 m and 700 m above the Kaena, respectively (Naish et al., 1998; Turner et al., 2005). An N–R transition just above the Mangaweka Mudstone in Watershed Road section was also interpreted as the Gauss–Matuyama boundary in the lower-resolution study of Sefton (2015). This is supported by previous mapping of the Rangitikei Group strata in the region (Naish and Kamp, 1995), biostratigraphic constraints, and the age and occurrence of the Eagle Hill Tephra (Tiri-2 correlative) in the lower part of the Watershed Road section.

The established magnetostratigraphy of the Turakina section also identifies the Gilbert–Gauss (3.58 Ma) R–N transition in the underlying Tangahoe Mudstone, 300 m below the Mammoth

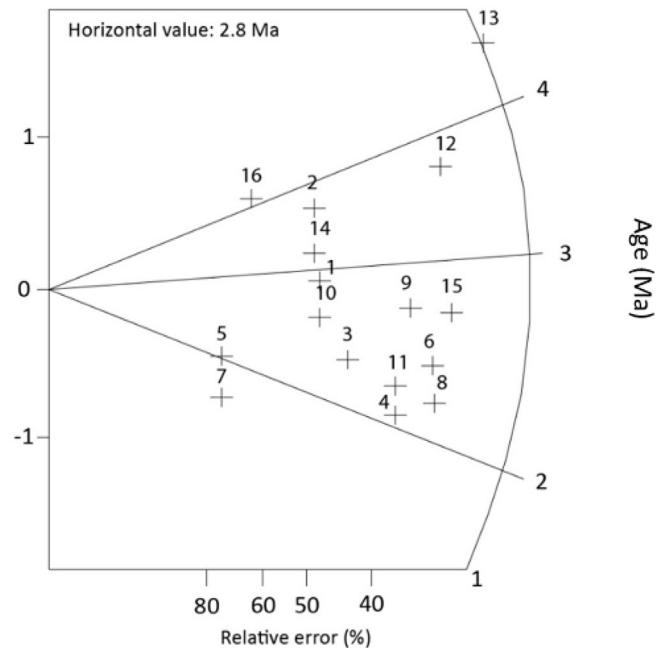


**Fig. 12.** Radial plot of single-grain zircon ages (1–16) from the Eagle Hill tephra yields an age of  $2.7 \pm 0.3$  Ma ( $1\sigma$ ). Raw data and detailed methodology is available in Sefton (2015). The y-axis displays the unit standard error. The fission-track analysis follows the external detector method (Hurford and Green, 1983). Ages were calculated using a zeta value of  $120 \pm 5$ . The probability of passing the chi-squared test ( $\chi^2$ ) is 95% suggesting the zircons analysed are from a single zircon population.

subchron (Turner et al., 2005).

The correlation of the polarity stratigraphy in the two drillcores with the GPTS (Ogg, 2012) as proposed by Tapia et al. (2018, in review) is further strengthened by the U–Pb age of  $3.12 \pm 0.18$  Ma obtained for the Siberia Tephra which occurs in Kaena Subchron in both the Turakina River section and ODP Site 1124C.

## 7. Discussion and conclusion

### 7.1. Orbitally-paced, glacial-interglacial shallow marine sedimentary cycles

We have established a cyclostratigraphic framework for the mid- to late Pliocene strata, and have identified 23 individual shallow-marine sedimentary cycles within the integrated drill core and outcrop data set, that can be correlated with individual cycles in benthic  $\delta^{18}\text{O}$  oxygen isotope records between 3.3 and 2.6 Ma (Fig. 4). A possible one-to-one correlation is made in Fig. 4, within the constraints of the chronostratigraphy, which establishes the relationship between the sedimentary cycles, frequency of the orbital forcing and the benthic oxygen isotope curve. While the water depths derived from benthic foraminiferal MAT generally display synchronous shallowing and deepening cycles with those based on lithofacies analysis, sequence stratigraphy and grainsize variations, they generally over-estimate relative amplitude of water depth changes suggested by the depositional environments interpreted from variations in lithofacies. This is not unexpected given the wide depth-ranges inhabited by key depth dependent genera. Previous applications of benthic foraminiferal census data to reconstruct water depths in Whanganui Basin Pliocene strata (e.g. Naish & Kamp, 1997a,b), had a restricted shoreline-proximal association which provided tighter constraints on shallowest water depths. This approach is less sensitive on the middle to outer shelf. Notwithstanding the lack of precision in amplitude, in the

absence of a significant northern hemisphere continental ice sheet prior to ~2.7 Ma (Maslin et al., 1998), amplitudes greater than ~30 m seem unlikely. Coeval, and broadly in-phase, fluctuations observed in the depositional environment interpretations, water depth proxies and climatic pollen indices, strengthen the linkage between regional climate and sea-level variability, and is consistent with a global climate driver on glacial-interglacial timescales. The cycles themselves, progressively deepen across a broad west-facing, wave-graded paleo-shelf transect from inner to outer shelf water depths, from the Rangitikei River Section to the Turakina section, respectively.

While our independent chronostratigraphic framework allows possible one-to-one correlations to be made between the sedimentary cycles and the high-resolution ODP Site 846 benthic  $\delta^{18}\text{O}$  record (Shackleton et al., 1995) through the mid-Pliocene interval (~3.3–3.0 Ma; with one exception – Cycle 12 in Fig. 4). This is not possible for the same interval in the benthic  $\delta^{18}\text{O}$  stack (Lisiecki and Raymo, 2005, Fig. 4), implying that the benthic stack is missing detail due to smoothing by the stacking methodology and/or poorly resolved individual  $\delta^{18}\text{O}$  time series over this interval. Cycles 1–14 within the mid-Pliocene Utiku Group appear to correspond to dominantly ~20 kyr-duration glacial-interglacial fluctuations in global sea-level (e.g. Meyers and Hinnov, 2010). The dominance of precession-forcing is not surprising as the Mammoth and Kaena Subchron's span a period of low obliquity variance and high precession variance, corresponding to a 1.2 Myr node in long-term obliquity and modulation of precession by high eccentricity due to the 400 kyr cycle. The dominance of precession does, however, imply a dominance of ice volume variability from one polar region over the other, likely the Antarctic based on evidence from a proximal ice-berg rafted debris record (Patterson et al., 2014), and a general lack of evidence for large northern hemisphere ice sheet variance at this time (Maslin et al., 1998). Cycles 15–23 in the late Pliocene Mangaweka Mudstone by contrast, correspond to dominantly ~40 kyr-duration glacial-interglacial fluctuations in sea level (Lisiecki and Raymo, 2005), perhaps in response to the development and relative dominance of developing continental ice sheets in the Northern Hemisphere after ~2.9 Ma (e.g. Raymo, 1994; Maslin et al., 1998).

## 7.2. Implications for reconstructing glacial-interglacial sea-level change

The continuous record of orbitally-paced water depth changes recorded by the Whanganui shallow-marine sedimentary cycles, described here, provides a unique opportunity to reconstruct the amplitude of glacial-interglacial fluctuations in GMSL during the warmer than present mid-Pliocene (3.3–3.0 Ma) and the late Pliocene (3.0–2.6 Ma), independent of the oxygen isotope record (c.f. Naish and Wilson, 2009; Miller et al., 2012).

A history of long-term tectonic subsidence during deposition of the Pliocene sediments, followed by uplift and exhumation during the late Quaternary, means it is not possible to register GMSL during interglacial highstands of the mid-Pliocene from Whanganui Basin to the present. Moreover, as outlined in the introduction of this paper, the influence of mantle dynamics on vertical land movement over the last 3 Ma renders peak Pliocene GMSL potentially unknowable (Rovere et al., 2014).

However, mantle dynamics have significantly less influence on glacial-interglacial timescales (Austermann et al., 2015). Therefore, by using a backstripping approach to remove the influence of sediment compaction and tectonic subsidence on relative sea-level changes (e.g. Kominz and Pekar, 2001; Miller et al., 2012), combined with correction for GIA (e.g. Raymo et al., 2011), it may be possible to reconstruct the amplitude of glacial-interglacial GMSL

changes during the mid-to late Pliocene from the Whanganui Basin record. This approach, together with an understanding of the frequency of sea-level change, could provide important insights to the relative contribution of polar ice sheets to GMSL and thus ice-sheet sensitivity under past climate conditions that were similar to those predicted for the coming centuries.

## Acknowledgements

The Royal Society of New Zealand, Marsden Grant 13 VUW 112, funded this research. The authors would like to acknowledge Webster Drilling and Exploration Ltd for the drilling operations and Alex Pyne and Darcy Mandeno of the Antarctic Research Centre, Science Drilling Office for drilling logistics support. We thank Frank Niessen of the Alfred Wegener Institute who provided the Geotek Multi-Sensor Core Logger, used to obtain the magnetic susceptibility log. Nick Pearce, Department of Geography & Earth Sciences, Aberystwyth University, UK, is thanked for his assistance in the acquisition of glass shard LA-ICP-MS data.

## References

- Alloway, B.V., Pillans, B.J., Naish, T.R., Westgate, J.A., 2004. Age and correlation of Ootaka tephra. Appendix in "Molluscan biostratigraphy of oxygen isotope stages of the last 2 million years in New Zealand". Part 1. Revised generic positions and recognition of warm- and cool-water migrants. *Beu, A.G. J. Roy. Soc. N. Z.* 34, 261–265.
- Alloway, B.V., Pillans, B.J., Carter, L., Naish, T.R., Westgate, J.A., 2005. Onshore-offshore correlation of Pleistocene rhyolitic eruptions from New Zealand: implications for TVZ eruptive history and paleoenvironmental reconstruction. *Quat. Sci. Rev.* 24 (14), 1601–1622.
- Anderton, P.W., 1981. Structure and evolution of the south wanganui basin, New Zealand. *N. Z. J. Geol. Geophys.* 24 (1), 39–63.
- Austermann, J., Pollard, D., Mitrovica, J.X., Moucha, R., Forte, A.M., DeConto, R.M., Rowley, D.B., Raymo, M.E., 2015. The impact of dynamic topography change on Antarctic ice sheet stability during the mid-Pliocene warm period. *Geology* 43 (10), 927–930.
- Beu, A.G., Maxwell, P.A., 1990. Cenozoic Mollusca of New Zealand. *N. Z. Geol. Surv. Paleontol. Bull.* 58, 518.
- Bunce, M., Worthy, T.H., Phillips, M.J., Holdaway, R.N., Willerslev, E., Haile, J., Shapiro, B., Schofield, R.P., Drummond, A., Kamp, P.J.J., Cooper, A., 2009. The evolutionary history of the extinct ratite moa and New Zealand Neogene paleogeography. *Proc. Natl. Acad. Sci. Unit. States Am.* 106 (49), 20646–20651. [www.pnas.org/cgi/doi/10.1073/pnas.0906660106](http://www.pnas.org/cgi/doi/10.1073/pnas.0906660106).
- Carter, L., Shane, P., Alloway, B., Hall, I.R., Harris, S.E., Westgate, J.A., 2003. Demise of one volcanic zone and birth of another – a 12 Ma Deep Ocean record of major rhyolitic eruptions from New Zealand. *Geology* 31, 493–496.
- Carter, L., Alloway, B., Shane, P., Westgate, J.A., 2004. Late Cenozoic major rhyolitic eruptions and dispersal – deep ocean records from off New Zealand. *N. Z. J. Geol. Geophys.* 47, 481–500.
- Cooper, R.A., Agterberg, F.P., Alloway, B.V., Beu, A.G., Campbell, H.J., Cooper, R.A., Crampton, J.S., Crouch, E.M., Crundwell, M.P., Graham, I.J., Hollis, C.J., Jones, C.M., Kamp, P.J.J., Mildenhall, D.C., Morgans, H.E.G., Naish, T.R., Raine, J.I., Roncaglia, L., Sadler, P.M., Schioler, P., Scott, G.H., Strong, C.P., Wilson, G.J., Wilson, G.S., 2004. The New Zealand Geological Timescale, vol. 22. *Intitue of Geological and Nuclear Sciences Monograph*, p. 284.
- DeConto, R.M., Pollard, D., Wilson, P.A., Pälike, H., Lear, C.H., Pagani, M., 2008. Thresholds for Cenozoic bipolar glaciation. *Nature* 455 (7213), 652.
- Dunbar, G.B., Barrett, P.J., 2005. Estimating paleobathymetry of wave-graded continental shelves from sediment texture. *Sedimentology* 52 (2), 253–269.
- Dutton, A., Carlson, A.E., Long, A.J., Milne, G.A., Clark, P.U., DeConto, R., Horton, B.P., Rahmstorf, S., Raymo, M.E., 2015. Sea-level rise due to polar ice-sheet mass loss during past warm periods. *Science* 349 (6244).
- Embry, A.F., 1993. Transgressive-regressive sequence stratigraphic analysis of the jurassic succession of the sverdrup basin, canadian arctic archipelago. *Can. J. Earth Sci.* 30, 301–320.
- Fleming, C.A., 1953. The geology of wanganui subdivision. *New Zealand Geological Survey bulletin* 52.
- Hammer, Ø., Harper, D.A.T., Ryan, P.D., 2001. PAST: paleontological statistics software package for education and data analysis. *Palaeontol. Electron.* 4 (1), 9.
- Hayward, B.W., 1986. A guide to paleoenvironmental assessment using New Zealand Cenozoic foraminiferal faunas. *N. Z. Geol. Surv. Rep. PAL* 109, 73.
- Hayward, B.W., Triggs, C.M., 2016. Using multi-foraminiferal-proxies to resolve the paleogeographic history of a lower Miocene, subduction-related, sedimentary basin (Waitemata Basin, New Zealand). *J. Foraminif. Res.* 46 (3), 285–313.
- Hayward, B.W., Grenfell, H.R., Reid, C.M., Hayward, K.A., 1999. Recent shallow-water benthic foraminifera: taxonomy, ecologic distribution, biogeography and use in paleoenvironmental assessment. *N. Z. Geol. Surv. Paleontol. Bull.* 75.



- Hunt, C.P., Moskowitz, B.M., Banerjee, S.K., 1995. Magnetic properties of rocks and minerals. *Rock physics & phase relations* 3, 189–204.
- Hurford, A.J., Green, P.F., 1983. The zeta age calibration of fission-track dating. *Chem. Geol.* 41, 285–317.
- Journeaux, T.D., 1995. Lithostratigraphy, Foraminiferal Paleocology and Sequence Stratigraphy of Middle Pliocene Marine Strata, Wanganui Basin, New Zealand. Unpublished M.Sc. thesis. University of Waikato.
- Journeaux, T.D., Kamp, P.J., Naish, T., 1996. Middle Pliocene cyclothem, Mangaweka region, wanganui basin, New Zealand: a lithostratigraphic framework. *N. Z. J. Geol. Geophys.* 39 (1), 135–149.
- Kamp, P.J., Journeaux, T.D., Morgans, H.E., 1998. Cyclostratigraphy of middle Pliocene middle shelf to upper slope strata, eastern Wanganui Basin (New Zealand): correlations to the deep sea isotope record. *Sediment. Geol.* 117 (3–4), 165–192.
- Kamp, P.J., Vonk, A.J., Bland, K.J., Hansen, R.J., Hendy, A.J., McIntyre, A.P., Ngatai, M., Cartwright, S.J., Hayton, S., Nelson, C.S., 2004. Neogene stratigraphic architecture and tectonic evolution of wanganui, king Country, and eastern taranaki basins, New Zealand. *N. Z. J. Geol. Geophys.* 47 (4), 625–644.
- Kominz, M.A., Pekar, S., 2001. Oligocene eustasy from two-dimensional sequence stratigraphic back-stripping. *Bull. Geol. Soc. Am.* 113, 291–304.
- Le Maitre, R.W., 1984. A proposal by the IUGS Subcommittee on the Systematics of Igneous Rocks for a chemical classification of volcanic rocks based on the total alkali silica (TAS) diagram: (on behalf of the IUGS Subcommittee on the Systematics of Igneous Rocks). *Aust. J. Earth Sci.* 31 (2), 243–255.
- Lisiecki, L.E., Raymo, M.E., 2005. A Pliocene-Pleistocene stack of 57 globally distributed benthic  $\delta^{18}O$  records. *Paleoceanography* 20 (1).
- Ludwig, K.R., Mundil, R., 2002. Extracting reliable U-Pb ages and errors from complex populations of zircons from Phanerozoic tuffs. In: *Geochimica et Cosmochimica Acta*. Pergamon-Elsevier Science Ltd, The Boulevard, Langford Lane, Kidlington, Oxford OX5 1gb, England (Vol. 66, No. 15 A, pp. A463–A463).
- Maslin, M.A., Li, X.S., Loutre, M.F., Berger, A., 1998. The contribution of orbital forcing to the progressive intensification of Northern Hemisphere glaciation. *Quat. Sci. Rev.* 17 (4–5), 411–426.
- Masson-Delmotte, V., Schulz, M., Abe-Ouchi, A., Beer, J., Ganopolski, A., González Rouco, J.F., Jansen, E., Lambeck, K., Luterbacher, J., Naish, T., Osborn, T., 2013. Information from paleoclimate archives. *Climate change* 383464, 2013.
- McGuire, D.M., 1989. Paleomagnetic Stratigraphy and Magnetic Properties of Pliocene Strata, Turakina River, North Island, New Zealand. Unpublished PhD thesis. Victoria University of Wellington.
- McIntyre, A.P., 2002. Geology of Mangapanian (Late Pliocene) Strata, Wanganui Basin: Lithostratigraphy, Palaeontology and Sequence Stratigraphy. Unpublished PhD thesis. University of Waikato.
- Meyers, S.R., Hinnov, L.A., 2010. Northern Hemisphere glaciation and the evolution of Plio-Pleistocene climate noise. *Paleoceanography* 25 (3).
- Milendhall, D.C., 2003. Deep-sea record of Pliocene and Pleistocene terrestrial palynomorphs from offshore eastern New Zealand (ODP Site 1123, Leg 181). *N. Z. J. Geol. Geophys.* 46 (3), 343–361.
- Milendhall, D.C., Hollis, C.J., Naish, T.R., 2004. Orbitally-influenced vegetation record of the mid-Pleistocene climate transition, offshore eastern New Zealand (ODP Leg 181, Site 1123). *Mar. Geol.* 205 (1–4), 87–111.
- Miller, K.G., Kominz, M.A., Browning, J.V., Wright, J.D., Mountain, G.S., Katz, M.E., Sugarman, P.J., Cramer, B.S., Christie-Blick, N., Pekar, S.F., 2005. The Phanerozoic record of global sea-level change. *Science* 310, 1293–1298.
- Miller, K.G., Wright, J.D., Browning, J.V., Kulpeck, A., Kominz, M., Naish, T.R., Cramer, B.S., Rosenthal, Y., Peltier, W.R., Sossian, S., 2012. High tide of the warm Pliocene: implications of global sea-level for Antarctic deglaciation. *Geology* 40 (5), 407–410.
- Moucha, R., Forte, A.M., Mitrovica, J.X., Rowley, D.B., Quéré, S., Simmons, N.A., Grand, S.P., 2008. Dynamic topography and long-term sea-level variations: there is no such thing as a stable continental platform. *Earth Planet. Sci. Lett.* 271 (1–4), 101–108.
- Müller, R.D., Sdrolias, M., Gaina, C., Steinberger, B., Heine, C., 2008. Long-term sea-level fluctuations driven by ocean basin dynamics. *Science (Washington, D.C.)* 319 (5868), 1357–1362.
- Naish, T., 1997. Constraints on the amplitude of late Pliocene eustatic sea-level fluctuations: new evidence from the New Zealand shallow-marine sediment record. *Geology* 25 (12), 1139–1142.
- Naish, T., Kamp, P.J., 1995. Pliocene-Pleistocene marine cyclothem, Wanganui Basin, New Zealand: a lithostratigraphic framework. *N. Z. J. Geol. Geophys.* 38 (2), 223–243.
- Naish, T., Kamp, P.J., 1997a. Sequence stratigraphy of sixth-order (41 ky) Pliocene–Pleistocene cyclothem, Wanganui basin, New Zealand: a case for the regressive systems tract. *Geol. Soc. Am. Bull.* 109 (8), 978–999.
- Naish, T., Kamp, P.J., 1997b. Foraminiferal depth palaeoecology of Late Pliocene shelf sequences and systems tracts, Wanganui Basin, New Zealand. *Sediment. Geol.* 110 (3–4), 237–255.
- Naish, T.R., Wilson, G.S., 2009. Constraints on the amplitude of Mid-Pliocene (3.6–2.4 Ma) eustatic sea-level fluctuations from the New Zealand shallow-marine sediment record. *Phil. Trans. Roy. Soc. Lond.: Math., Phys. Eng. Sci.* 367 (1886), 169–187.
- Naish, T., Kamp, P.J., Alloway, B.V., Pillans, B., Wilson, G.S., Westgate, J.A., 1996. Integrated tephrochronology and magnetostratigraphy for cyclothem marine strata, Wanganui Basin: implications for the Pliocene-Pleistocene boundary in New Zealand. *Quat. Int.* 34, 29–48.
- Naish, T.R., Abbott, S.T., Alloway, B.V., Beu, A.G., Carter, R.M., Edwards, A.R., Journeaux, T.D., Kamp, P.J., Pillans, B.J., Saul, G., Woolfe, K.J., 1998. Astronomical calibration of a southern hemisphere Plio-Pleistocene reference section, Wanganui Basin, New Zealand. *Quat. Sci. Rev.* 17 (8), 695–710.
- Ogg, J.G., 2012. Geomagnetic polarity time scale. In: *Gradstein, F.M., Ogg, J.G., Schmitz, M., Ogg, G. (Eds.), The Geologic Time Scale 2012*. Elsevier, pp. 85–113.
- Patterson, M.O., 2014. The Response of Antarctic Ice Volume, Global Sea-level and Southwest Pacific Ocean Circulation to Orbital Variations during the Pliocene to Early Pleistocene. Unpublished PhD thesis. Victoria University of Wellington.
- Patterson, M.O., McKay, R., Naish, T., Escutia, C., Jimenez-Espejo, F.J., Raymo, M.E., Meyers, S.R., Tauxe, L., Brinkhuis, H., Expedition, I.O.D.P., Klaus, A., 2014. Orbital forcing of the East Antarctic ice sheet during the Pliocene and Early Pleistocene. *Nat. Geosci.* 7 (11), 841.
- Pillans, B., Alloway, B., Naish, T., Westgate, J., Abbott, S., Palmer, A., 2005. Silicic tephras in Pleistocene shallow-marine sediments of Wanganui Basin, New Zealand. *J. Roy. Soc. N. Z.* 35 (1–2), 43–90.
- Pulford, A., Stern, T., 2004. Pliocene exhumation and landscape evolution of central North Island, New Zealand: the role of the upper mantle. *J. Geophys. Res.: Earth Surf.* 109 (F1).
- Raine, J.L., Beu, A.G., Boyes, A.F., Campbell, H.J., Cooper, R.A., Crampton, J.S., Crundwell, M.P., Hollis, C.J., Morgans, H.E.G., Mortimer, N., 2015. New Zealand geological timescale NZGT 2015/1. *N. Z. J. Geol. Geophys.* 58 (4), 398–403.
- Raymo, M.E., 1994. The initiation of Northern Hemisphere glaciation. *Annu. Rev. Earth Planet. Sci.* 22 (1), 353–383.
- Raymo, M.E., Mitrovica, J.X., O'Leary, M.J., DeConto, R.M., Hearty, P.J., 2011. Departures from eustasy in Pliocene sea-level records. *Nat. Geosci.* 4, 328–332.
- Rohling, E.J., Foster, G.L., Grant, K.M., Marino, G., Roberts, A.P., Tamsiea, M.E., Williams, F., 2014. Sea-level and deep-sea-temperature variability over the past 5.3 million years. *Nature* 508 (7497), 477.
- Rovere, A., Raymo, M.E., Mitrovica, J.X., Hearty, P.J., O'Leary, M.J., Inglis, J.D., 2014. The Mid-Pliocene sea-level conundrum: glacial isostasy, eustasy and dynamic topography. *Earth Planet. Sci. Lett.* 387, 27–33.
- Sagar, M.W., Palin, J.M., 2011. Emplacement, metamorphism, deformation and affiliation of mid-Cretaceous orthogneiss from the Paparoa Metamorphic Core Complex lower-plate, Charleston, New Zealand. *N. Z. J. Geol. Geophys.* 54 (3), 273–289.
- Saul, G., Naish, T.R., Abbott, S.T., Carter, R.M., 1999. Sedimentary cyclicity in the marine Pliocene-Pleistocene of the Wanganui basin (New Zealand): sequence stratigraphic motifs characteristic of the past 2.5 my. *Geol. Soc. Am. Bull.* 111 (4), 524–537.
- Sefton, J.P., 2015. An Assessment of the Influence of Orbital Forcing on Late Pliocene Global Sea-level Using a Shallow-marine Sedimentary Record from the Wanganui Basin. Unpublished MSc thesis, Victoria University of Wellington, New Zealand.
- Shackleton, N.J., Crowhurst, S., Hagelberg, T., Pisias, N.G., Schneider, D.A., 1995. A new late Neogene time scale: application to Leg 138 sites. In: *Proc. ODP, Sci. Results*, Vol. 138, pp. 73–101.
- Stern, T.A., Quinlan, G.M., Holt, W.E., 1992. Basin formation behind an active subduction zone: three-dimensional flexural modelling of Wanganui Basin, New Zealand. *Basin Res.* 4 (3–4), 197–214.
- Stern, T., Houseman, G., Salmon, M., Evans, L., 2013. Instability of a lithospheric step beneath western North Island, New Zealand. *Geology* 41 (4), 423–426.
- Stevens, M.T., 2010. Miocene and Pliocene Silicic Coromandel Volcanic Zone Etphras from ODP Site 1124-C: Petrogenetic Applications and Temporal Evolution. Unpublished MSc thesis. Victoria University of Wellington.
- Tapia, C.A., Grant, G.R., Turner, G.M., Sefton, J.P., Ohneiser, C., Naish, T.R., Dunbar, G.B., 2018. High-resolution magnetostratigraphy of mid-Pliocene (~3.3–3.0 Ma) shallow-marine sediments, Whanganui Basin, New Zealand. *Geophys. J. Int.* (in review).
- Trewick, S.A., Bland, K.J., 2012. Fire and slice: palaeogeography for biogeography at New Zealand's North Island/South Island juncture. *J. Roy. Soc. N. Z.* 42 (3), 153–183.
- Turner, G.M., Kamp, P.J., McIntyre, A.P., Hayton, S., McGuire, D.M., Wilson, G.S., 2005. A coherent middle Pliocene magnetostratigraphy, Wanganui Basin, New Zealand. *J. Roy. Soc. N. Z.* 35 (1–2), 197–227.